NON-OSCILLATORY HIERARCHICAL RECONSTRUCTION FOR CENTRAL AND FINITE VOLUME SCHEMES

YINGJIE LIU, CHI-WANG SHU, EITAN TADMOR, AND MENGPING ZHANG

Abstract. This is the continuation of the paper "central discontinuous Galerkin methods on overlapping cells with a non-oscillatory hierarchical reconstruction" by the same authors. The hierarchical reconstruction introduced therein is applied to central schemes on overlapping cells and to finite volume schemes on non-staggered grids. This takes a new finite volume approach for approximating non-smooth solutions. A critical step for high order finite volume schemes is to reconstruct a non-oscillatory high degree polynomial approximation in each cell out of nearby cell averages. In the paper this procedure is accomplished in two steps: first to reconstruct a high degree polynomial in each cell by using e.g., a central reconstruction, which is easy to do despite the fact that the reconstructed polynomial could be oscillatory; then to apply the hierarchical reconstruction to remove the spurious oscillations while maintaining the high resolution. All numerical computations for systems of conservation laws are performed without characteristic decomposition. In particular, we demonstrate that this new approach can generate essentially non-oscillatory solutions even for 5th order schemes without characteristic decomposition.

Contents

Date: October 30, 2006.

Key words and phrases. Central scheme, discontinuous Galerkin method, ENO scheme, finite volume scheme, MUSCL scheme, TVD scheme.

Acknowledgment. The research of Y. Liu was supported in part by NSF grant DMS-0511815. The research of C.-W. Shu was supported in part by the Chinese Academy of Sciences while this author was visiting the University of Science and Technology of China (grant 2004-1-8) and the Institute of Computational Mathematics and Scientific/Engineering Computing. Additional support was provided by ARO grant W911NF-04-1-0291 and NSF grant DMS-0510345. The research of E. Tadmor was supported in part by NSF grant 04-07704 and ONR grant N00014-91-J-1076. The research of M. Zhang was supported in part by the Chinese Academy of Sciences grant 2004-1-8.

1. Introduction

Finite volume schemes are powerful numerical methods for solving nonlinear conservation laws and related equations. It evolves only cell averages of a solution over time and is locally conservative. The first-order Godunov and Lax-Friedrichs (LxF) schemes are, respectively, the forerunners for the large class of upwind and central high-resolution finite volume schemes. However, the cell average of a solution in a cell contains too little information. In order to obtain higher order accuracy, neighboring cell averages must be used to reconstruct an approximate polynomial solution in each cell. This reconstruction procedure is the key step for many high-resolution schemes. We mention here the notable examples of the high-resolution upwind FCT, MUSCL, TVD, PPM, ENO, and WENO schemes [6, 40, 13, 11, 14, 25] and this list is far from being complete. The central scheme of Nessyahu and Tadmor (NT) [29] provides a second-order generalization of the staggered LxF scheme. It is based on the same piece-wise linear reconstructions of cell averages used with upwind schemes, yet the solution of (approximate) Riemann problems is avoided. High resolution generalizations of the NT scheme were developed since the 90s as the class of central schemes in e.g. [34, 2, 18, 16, 26, 4, 19, 1, 20, 21, 24, 27] and the list is far from being complete. The second order MUSCL, high order ENO and WENO reconstructions are effective non-oscillatory reconstruction methods which select the smoothest possible nearby cell averages to reconstruct the approximate polynomial solution in a cell, and can be used for uniform or unstructured meshes in multi space dimensions. In Hu and Shu [15], WENO schemes for triangular meshes are developed, and in Arminjon and St-Cyr [1], central scheme with the MUSCL reconstruction is extended to unstructured staggered meshes. When reconstruction order becomes higher, characteristic decomposition is usually necessary to reduce spurious oscillations for systems of conservation laws. Characteristic decomposition locally creates larger smooth area for polynomial reconstruction by separating discontinuities into different characteristic fields. Comparisons of high order WENO and central schemes with or without characteristic decomposition are studied in Qiu and Shu [30]. As the formal order of accuracy becomes higher, e.g. 5th order, spurious oscillations become evident for both schemes without characteristic decomposition (for the Lax problem), even though oscillations in central schemes tend to be smaller.

In a series of works by Cockburn and Shu *et al.* ([8, 9, 10] *etc*), discontinuous Galerkin (DG) methods are developed for nonlinear conservation laws and related equations. Compared to finite volume schemes, DG stores and evolves every polynomial coefficient in a cell over time. Therefore there is no need to use information in non local cells to achieve high order accuracy. When the solution is non smooth, similar to finite volume schemes, DG also needs a nonlinear limiting procedure to remove spurious oscillations in order to maintain the high resolution near discontinuities. In Cockburn and Shu [8], a limiting procedure is introduced for DG which compares the variation of the polynomial solution in a cell to the variation of neighboring cell averages to detect the non-smoothness. Nonlinear part of the polynomial is truncated in non smooth region. The limiting procedure is proved to be total variation bounded (TVB). In [5], Biswas, Devine and Flaherty develop a moment limiter which takes into account higher degree terms. In Qiu and Shu [32, 31], the WENO and Hermite WENO reconstructions are developed as limiters for DG. The list of new developments for limiting in DG is growing and is far from being complete. In [28], we develop a central discontinuous Galerkin (DG) method on overlapping cells and a non-oscillatory limiting procedure. The so-called hierarchical reconstruction is related to [5] and to the early work [8]. This limiting procedure requires only linear reconstructions at each stage using information from adjacent cells and can be implemented (at least in theory) for any shape of cells. Therefore it could be useful for unstructured meshes or even for dynamically moving meshes (e.g. Tang and Tang [39]), although we do not pursue too far in unstructured meshes here. Another distinguished feature of the hierarchical reconstruction is that it does not use characteristic decomposition even in high order, which we are going to study further in this work by using the finite volume framework.

We develop a new finite volume approach by using the hierarchical reconstruction introduced in [28]. Instead of directly reconstructing a non-oscillatory polynomial solution in each cell by using the smoothest neighboring cell averages, we break the task into two steps. First we use a central finite volume reconstruction (or other convenient methods) to reconstruct a high degree polynomial in each cell. These polynomials are not necessarily non-oscillatory, therefore the reconstruction can be done in a simple way. Then we apply the hierarchical reconstruction to the piece-wise polynomial solution in order to remove the possible spurious oscillations while keeping the high order accuracy. With this approach, we demonstrate that both central schemes on overlapping cells and finite volume schemes on non-staggered meshes do not have significant spurious oscillations without characteristic decomposition, for formal order of accuracy as high as 5th order, although there are still some small overshoots and undershoots at discontinuities of the solution.

This paper is organized as follows. In Sec. 2, we briefly introduce central schemes on overlapping cells. Finite volume schemes on non-staggered grids are described in Sec. 3. Various central reconstructions for overlapping cells and non-staggered grids are discussed within these sections. In Sec. 4, we discuss the non-oscillatory hierarchical reconstruction procedure for these schemes. Numerical examples are presented in Sec. 5.

2. Central Schemes on Overlapping Cells

Consider the scalar one dimensional conservation law

$$\frac{\partial u}{\partial t} + \frac{\partial f(u)}{\partial x} = 0, \qquad (x,t) \in \mathcal{R} \times (0,T). \tag{2.1}$$

Set $\{x_i := x_0 + i\Delta x\}$, let $C_{i+1/2} := [x_i, x_{i+1})$ be a uniform partition of $\mathcal{R}$ and let $\{\overline{U}^n_{i+1/2}\}$ denote the set of approximate cell averages $\overline{U}^n_{i+1/2} \approx (1/\Delta x)\int_{C_{i+1/2}} u(x,t^n)dx$. Similarly, we set $D_i := [x_{i-1/2}, x_{i+1/2})$ as the dual partition and let $\{\overline{V}^n_i\}$ denote the corresponding set of approximate cell average $\overline{V}^n_i \approx (1/\Delta x)\int_{D_i} u(x,t^n)dx$. Starting with these two piecewise-constant approximation[1],

$$\sum_i \overline{U}^n_{i+1/2}\mathbf{1}_{C_{i+1/2}}(x) \quad \text{and} \quad \sum_i \overline{V}^n_i \mathbf{1}_{D_i}(x),$$

we proceed to compute our approximate solution at the next time level, $t^{n+1} := t^n + \Delta t^n$. To this end, we reconstruct two higher-order piecewise-polynomial approximations,

$$U^n(x) = \sum_i U_{i+1/2}(x)\mathbf{1}_{C_{i+1/2}}(x) \quad \text{and} \quad V^n(x) = \sum_i V_i(x)\mathbf{1}_{D_i}(x)$$

with breakpoints at $x_i, i = 0, \pm1, \pm2, \cdots$, and respectively, at $x_{i+1/2}, i = 0, \pm1, \pm2, \cdots$. These piecewise-polynomials should be conservative in the sense that $\int_{C_{j+1/2}} U^n(x)dx = \Delta x\overline{U}^n_{j+1/2}$ and $\int_{D_j} V^n(x)dx = \Delta x\overline{V}^n_j$ for all j's. Following Nessyahu and Tadmor [29], the central scheme associated with these piecewise-polynomials reads

$$\overline{V}^{n+1}_i = \frac{1}{\Delta x}\int_{D_i} U^n(x)dx - \frac{\Delta t^n}{\Delta x}\Big[f(U^{n+\frac{1}{2}}(x_{i+1/2})) - f(U^{n+\frac{1}{2}}(x_{i-1/2}))\Big], \tag{2.2a}$$

$$\overline{U}^{n+1}_{i+1/2} = \frac{1}{\Delta x}\int_{C_{i+1/2}} V^n(x)dx - \frac{\Delta t^n}{\Delta x}\Big[f(V^{n+\frac{1}{2}}(x_{i+1})) - f(V^{n+\frac{1}{2}}(x_i))\Big]. \tag{2.2b}$$

To guarantee second-order accuracy, the right-hand-sides of (2.2a), (2.2b) require the approximate values of $U^{n+\frac{1}{2}}(x_{j+1/2}) \approx u(x_{j+1/2}, t^{n+\frac{1}{2}})$ and $V^{n+\frac{1}{2}}(x_j) \approx u(x_j, t^{n+\frac{1}{2}})$ to be evaluated at the midpoint

[1]Here and below, $\mathbf{1}_\Omega(x)$ denotes the characteristic function of Ω

$t + \Delta t^n/2$. Replacing the midpoint rule with higher order quadratures, yields higher order accuracy, e.g., [26, 4].

The central Nessyahu-Tadmor (NT) scheme (2.2) and its higher-order generalizations provide effective high-resolution "black-box" solvers to a wide variety of nonlinear conservation laws. When Δt is very small, however, e.g., with $\Delta t = \mathcal{O}\big((\Delta x)^2\big)$ as required by the CFL condition for convection-diffusion equations for example, the numerical dissipation of the NT schemes becomes excessively large. The excessive dissipation is due to the staggered grids where at each time-step, cell averages are shifted $\Delta x/2$-away from each other. To address this difficulty, Kurganov and Tadmor, [21], suggested to remove this excessive dissipation by using staggered grids which are shifted only $\mathcal{O}(\Delta t)$-away from each other. This amounts to using control volumes of width $\mathcal{O}(\Delta t)$ so that the resulting schemes admits semi-discrete limit as $\Delta t \to 0$, the so called "central-upwind" schemes introduced in [21] and further generalized in [20]. Liu [27] introduced another modification of the NT scheme which removes its $\mathcal{O}(1/\Delta t)$ dependency of numerical dissipation. In this approach, one takes advantage of the *r*edundant representation of the solution over overlapping cells, $\overline{V}_i^n$ and $\overline{U}_{i+1/2}^n$. The idea is to use a $\mathcal{O}(\Delta t)$-dependent weighted average of $\overline{U}_{i+1/2}^n$ and $\overline{V}_i^n$. To simplify our discussion, we momentarily give up on second-order accuracy in time, setting $U^{n+\frac{1}{2}} = U^n$ and $V^{n+\frac{1}{2}} = V^n$ in (2.2a) and (2.2b). The resulting first-order forward-Euler formulation of the new central scheme reads

$$\overline{V}_i^{n+1} = \theta\Big(\frac{1}{\Delta x}\int_{D_i} U^n(x)dx\Big) + (1-\theta)\overline{V}_i^n - \frac{\Delta t^n}{\Delta x}\Big[f(U^n(x_{i+1/2})) - f(U^n(x_{i-1/2}))\Big], \tag{2.3a}$$

$$\overline{U}_{i+1/2}^{n+1} = \theta\Big(\frac{1}{\Delta x}\int_{C_{i+1/2}} V^n(x)dx\Big) + (1-\theta)\overline{U}_{i+1/2}^n - \frac{\Delta t^n}{\Delta x}\Big[f(V^n(x_{i+1})) - f(V^n(x_i))\Big]. \tag{2.3b}$$

Here $\theta := \Delta t^n/\Delta\tau^n$ where $\Delta\tau^n$ is an upper bound for the time step, dictated by the CFL condition. Note that when $\theta = 1$, (2.3a), (2.3b) is reduced to the first-order, forward-Euler-based version of the NT scheme (2.2a), (2.2b). The reduced dissipation allows us to pass to a semi-discrete formulation: subtracting $\overline{V}_i^n$ and $\overline{U}_{i+1/2}^n$ from both sides, multiplying by $\frac{1}{\Delta t^n}$, and then passing to the limit as $\Delta t^n \to 0$ we end up with

$$\frac{d}{dt}\overline{V}_i(t^n) = \frac{1}{\Delta\tau^n}\left(\frac{1}{\Delta x}\int_{D_i} U^n(x)dx - \overline{V}_i^n\right) - \frac{1}{\Delta x}\big[f(U^n(x_{i+1/2})) - f(U^n(x_{i-1/2}))\big], \tag{2.4a}$$

$$\frac{d}{dt}\overline{U}_{i+1/2}(t^n) = \frac{1}{\Delta\tau^n}\left(\frac{1}{\Delta x}\int_{C_{i+1/2}} V^n(x)dx - \overline{U}_{i+1/2}^n\right) - \frac{1}{\Delta x}\big[f(V^n(x_{i+1})) - f(V^n(x_i))\big]. \tag{2.4b}$$

The spatial accuracy of the semi-discrete central scheme (2.4) is dictated by the order the reconstruction $U^n(x)$ and $V^n(x)$. The SSP Runge-Kutta methods [37, 12] yield the matching high-order discretization in time. There are two reconstruction procedures for overlapping cells: one is the standard procedure to reconstruct the two classes of cell averages $\{\overline{V}_i^n : i = 0, \pm1, \pm2, \cdots\}$ and $\{\overline{U}_{i+1/2}^n : i = 0, \pm1, \pm2, \cdots\}$; the other couples these two classes for reconstruction of the final representation of the solution. Thus, this approach is redundant. At the same time, numerical examples in [27] have shown that by coupling the reconstructions, redundancy does provide improved resolution when compared with the one-cell average evolution approach of Godunov-type schemes.

2.1. **Extension to Multi Dimensions.** Consider the scalar conservation law

$$\frac{\partial u}{\partial t} + \nabla_{\mathbf{x}} \cdot \mathbf{f}(\mathbf{u}) = 0, \qquad (\mathbf{x}, t) \in \mathcal{R}^d \times (0, T), \tag{2.5}$$

where $\mathbf{u} = (u_1, \ldots, u_m)^\top$. For simplicity, assume a uniform staggered rectangular mesh depicted in figure 1 for the 2D case. Let $\{C_{I+1/2}\}$, $I = (i_1, i_2, \cdots, i_d)$ be a partition of R^d into uniform square cells depicted by solid lines in figure 1 and tagged by their cell centroids at the *h*alf integers, $\mathbf{x}_{I+1/2} :=$

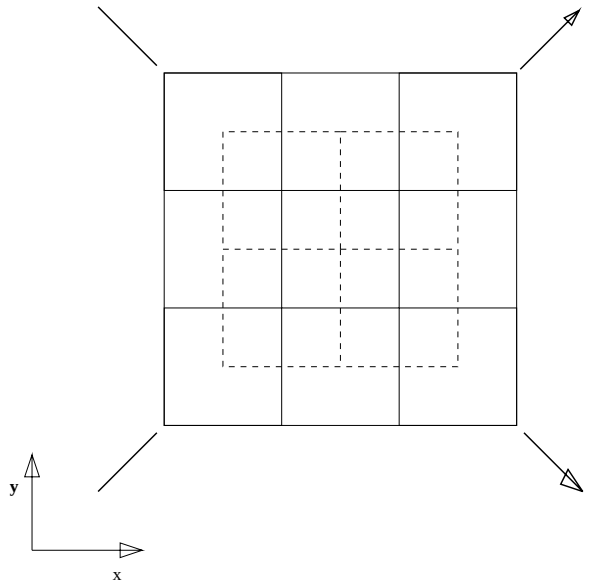

Figure 1: 2D overlapping cells by collapsing the staggered dual cells on two adjacent time levels to one time level;

$(I+1/2)\Delta x$. Let $\overline{U}_{I+1/2}(t)$ be the numerical cell average approximating $(1/|C_{I+1/2}|)\int_{C_{I+1/2}} u(\mathbf{x},t)d\mathbf{x}$, in particular, $\overline{U}^n_{I+1/2} = \overline{U}_{I+1/2}(t^n)$. Let $\{D_I\}$ be the dual mesh which consists of a $\Delta x/2$- shift of the $C_{I+1/2}$'s depicted by dash lines in figure 1. Let $\mathbf{x}_I$ be the cell centroid of the cell D_I. Let $\overline{V}_I(t)$ be the numerical cell average approximating $(1/|D_I|)\int_{D_I} u(\mathbf{x},t)d\mathbf{x}$. The semi-discrete central scheme on overlapping cells can written as follows [27]

$$\frac{d}{dt}\overline{U}_{I+1/2}(t^n) = \frac{1}{\Delta\tau^n}\left(\frac{1}{|C_{I+1/2}|}\int_{C_{I+1/2}} V^n(\mathbf{x})d\mathbf{x} - \overline{U}^n_{I+1/2}\right) - \frac{1}{|C_{I+1/2}|}\int_{\partial C_{I+1/2}} \mathbf{f}(V^n(\mathbf{x}))\cdot\mathbf{n}ds, \tag{2.6a}$$

$$\frac{d}{dt}\overline{V}_I(t^n) = \frac{1}{\Delta\tau^n}\left(\frac{1}{|D_I|}\int_{D_I} U^n(\mathbf{x})d\mathbf{x} - \overline{V}^n_I\right) - \frac{1}{|D_I|}\int_{\partial D_I} \mathbf{f}(U^n(\mathbf{x}))\cdot\mathbf{n}ds. \tag{2.6b}$$

2.2. **Central Finite Volume Reconstructions.** Standard non-oscillatory finite volume reconstruction procedures such as ENO [14, 37] or WENO [25, 17] *etc*, choose the smoothest possible nearby cell cell averages to construct a non-oscillatory high order polynomial in a cell. Here we take a different approach: first construct a polynomial of the desired degree (which could be oscillatory) in each cell by using a central finite volume reconstruction (or other finite volume reconstructions); then apply the hierarchical reconstruction ([28], also described in Sec. 4) to remove the possible spurious oscillations while keeping the formal order of accuracy of the central finite volume reconstruction. For systems of conservation laws, we use a component-wise extension of (2.6) without characteristic decomposition. One of the special properties of this new approach is that we observe essentially non-oscillatory numerical solutions near discontinuities even for 5th order schemes without characteristic decomposition, though small overshoots do occur. Conventional methods without characteristic decomposition tend to generate more evident artifacts or oscillations beyond 3rd order formal accuracy, see e.g. [30].

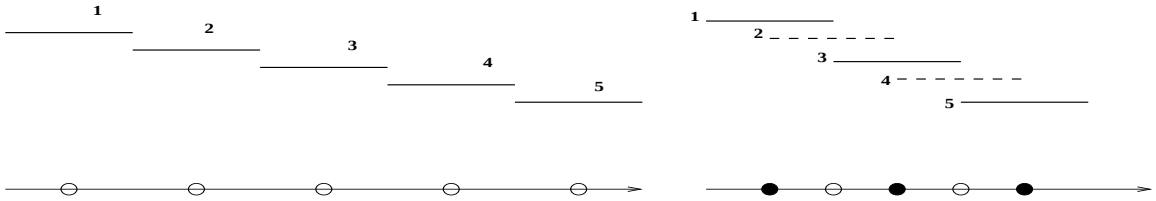

Figure 2: Left: 1D non-staggered cells. Right: 1D overlapping cells. To construct a 4th degree polynomial for cell 3 involves cell $1, 2, 4, 5$ and 3.

2.2.1. *Central Reconstructions in* 1*D.* For convenience, we use a slightly different notation from previous subsections and assume the approximate cell average $\overline{U}_i$ is given at the overlapping cell C_i, with cell center x_i, $i = 1, 2, \cdots, 5$, see figure 2 right. In order to construct a quadratic polynomial $U_3(x - x_3) = U_3(0) + U_3'(0)(x - x_3) + \frac{1}{2}U_3''(0)(x - x_3)^2$ in cell C_3, one can solve the following linear system

$$\frac{1}{|C_i|}\int_{C_i} U_3(x - x_3)dx = \overline{U}_i, \quad i = 2, 3, 4.$$

Similarly, in order to construct a 4th degree polynomial $U_3(x-x_3) = U_3(0)+U_3'(0)(x-x_3)+\frac{1}{2}U_3''(0)(x-x_3)^2 + \frac{1}{3!}U_3^{(3)}(0)(x - x_3)^3 + \frac{1}{4!}U_3^{(4)}(0)(x - x_3)^4$ in cell C_3, one solves the following linear system

$$\frac{1}{|C_i|}\int_{C_i} U_3(x - x_3)dx = \overline{U}_i, \quad i = 1, 2, 3, 4, 5.$$

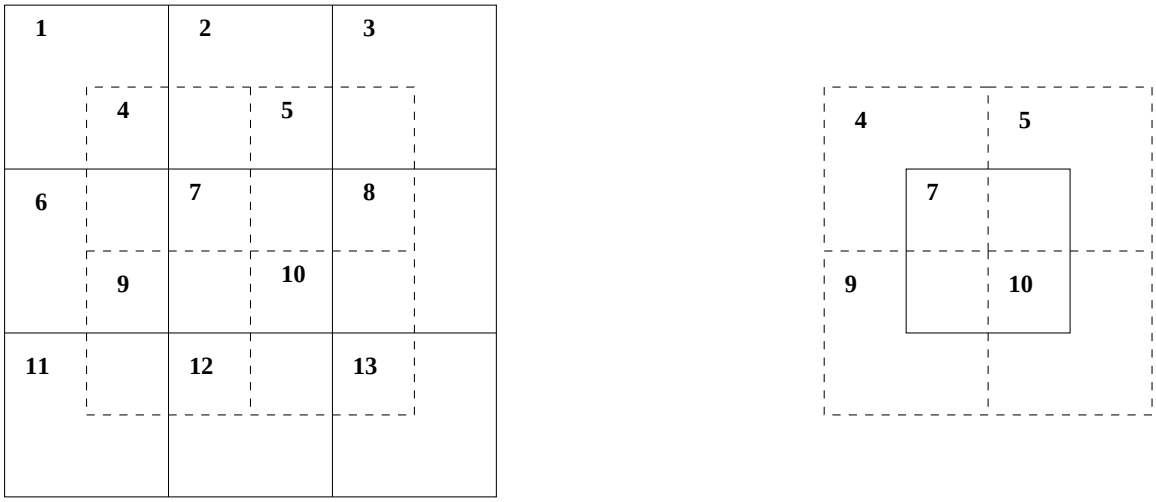

Figure 3: 2D overlapping cells. Left: to construct a cubic polynomial in cell 7 involves cell averages from 13 adjacent overlapping cells. Right: non-oscillatory hierarchical reconstruction for cell 7 involves only polynomials in overlapping cell $4, 5, 9, 10$ and 7.

2.2.2. *A Central* 4*th Order Reconstruction in* 2*D.* Assume that the approximate cell average $\overline{U}_i$ is given at the overlapping cell C_i, with cell centroid $\mathbf{x}_i$, $i = 1, 2, \cdots, 13$, see figure 3 left. In order to construct a cubic polynomial $U_7(\mathbf{x} - \mathbf{x}_7)$ in cell C_7, we need 10 nearby cell averages. One could certainly pick a suitable set of 10 cells (including cell C_7) out of the 13 cells adjacent to cell C_7. Here we take a more systematic least square approach following [3, 15],

$$\min\{\sum_{1\le i\le 13, i\neq 7}[\frac{1}{|C_i|}\int_{C_i} U_7(\mathbf{x} - \mathbf{x}_7)d\mathbf{x} - \overline{U}_i]^2\}, \text{ subject to } \frac{1}{|C_7|}\int_{C_7} U_7(\mathbf{x} - \mathbf{x}_7)d\mathbf{x} = \overline{U}_7.$$

This can be solved by the method of Lagrangian multiplier. Let

$$\mathcal{G} = \sum_{1\le i\le 13, i\neq 7} [\frac{1}{|C_i|}\int_{C_i} U_7(\mathbf{x}-\mathbf{x}_7)d\mathbf{x} - \overline{U}_i]^2 + \alpha[\frac{1}{|C_7|}\int_{C_7} U_7(\mathbf{x}-\mathbf{x}_7)d\mathbf{x} - \overline{U}_7],$$

then $\bigtriangledown\mathcal{G} = 0$ yields a linear system. The coefficient matrix of the linear system is invariant from cell to cell for the uniform mesh. Therefore the least square problem is solved only once and the inverse of the coefficient matrix can be stored for calculating a cubic polynomial in each cell.

We also apply this reconstruction to an irregular staggered mesh such that for one class of cells, $\Delta x = \Delta y = h$ in the upper half domain and $\Delta x = 2\Delta y = h$ in the lower half domain .

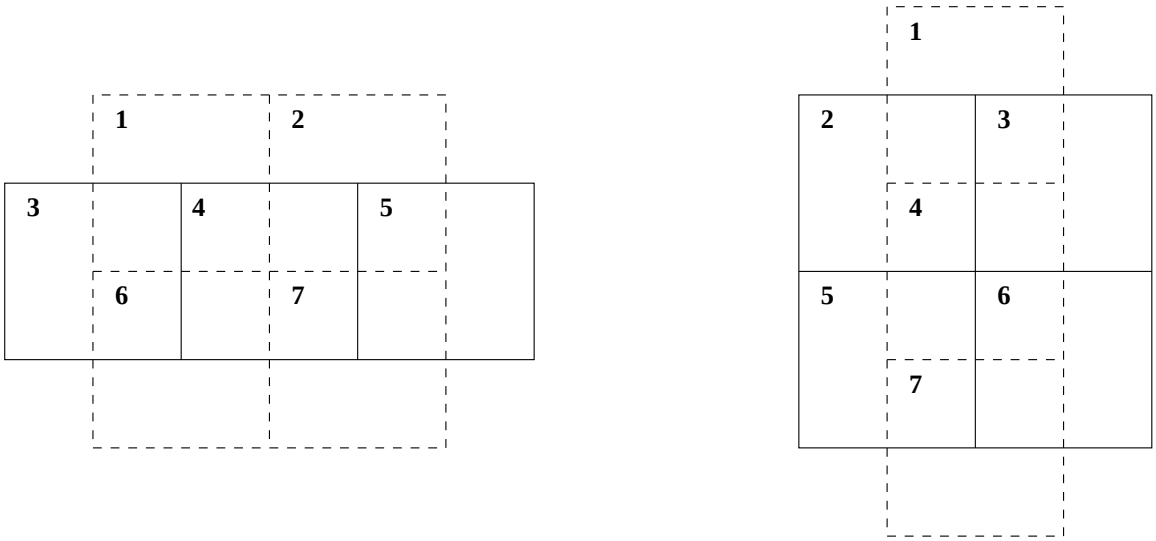

Figure 4: 2D overlapping cells. Left: to construct a quadratic polynomial in cell 4 (belongs to one class) involves cell averages from 7 adjacent overlapping cells. Right: to construct a quadratic polynomial in cell 4 (belongs to the dual class) involves different set of cells.

2.2.3. *A Central 3rd Order Reconstruction in 2D.* The similar least square strategy can also be used to reconstruct a quadratic polynomial in each cell. However, we want to try a different reconstruction method here. It is non symmetric and is slightly different for the two classes of overlapping cells, see figure 4. On the left, suppose cell C_4 belongs to a cell class of the two overlapping cell classes, we can reconstruct a quadratic polynomial $U_4(\mathbf{x}-\mathbf{x}_4)$ in cell C_4 by solving

$$\frac{1}{|C_i|}\int_{C_i} U_4(\mathbf{x}-\mathbf{x}_4)d\mathbf{x} = \overline{U}_i, \quad i = 1, 2, 4, 6, 7,$$

and

$$\int_{C_3\cup C_5} U_4(\mathbf{x}-\mathbf{x}_4)d\mathbf{x} = \overline{U}_3|C_3| + \overline{U}_5|C_5|.$$

On the right of figure 4, suppose cell C_4 belongs to the dual cell class, we can reconstruct a quadratic polynomial $U_4(\mathbf{x}-\mathbf{x}_4)$ in cell C_4 by solving

$$\frac{1}{|C_i|}\int_{C_i} U_4(\mathbf{x}-\mathbf{x}_4)d\mathbf{x} = \overline{U}_i, \quad i = 2, 3, 4, 5, 6,$$

and

$$\int_{C_1\cup C_7} U_4(\mathbf{x}-\mathbf{x}_4)d\mathbf{x} = \overline{U}_1|C_1| + \overline{U}_7|C_7|.$$

Even though the reconstruction is non-symmetric for each class of cells, the combination of them has no preference in each coordinate direction.

3. Finite Volume Schemes

The new finite volume approach can also be applied to non-staggered meshes. We first study a 5th order finite volume scheme on the 1D uniform grid for equation (2.1). Recall that $\{x_i := x_0 + i\Delta x\}$, $C_{i+1/2} := [x_i, x_{i+1})$ is a uniform partition of $\mathcal{R}$, and $\{\overline{U}^n_{i+1/2}\}$ (or $\{\overline{U}_{i+1/2}(t^n)\}$) denotes the set of approximate cell averages $\overline{U}^n_{i+1/2} \approx (1/\Delta x)\int_{C_{i+1/2}} u(x,t^n)dx$. Out of these approximate cell averages, one can apply a conservative finite volume reconstruction to obtain a piece-wise polynomial $U^n(x)$ (or $U(x,t^n)$) with breaking points at $\{x_i\}$. Then the semi-discrete finite volume formulation can be written as follows (see e.g. [36] for more details)

$$\frac{d}{dt}\overline{U}_{i+1/2}(t^n) = -\frac{1}{\Delta x}(\hat{f}^n_{i+1} - \hat{f}^n_i), \tag{3.1}$$

where $\hat{f}^n_i$ is the numerical flux defined by $\hat{f}^n_i = h(U^n(x_i-), U^n(x_i+))$. Here we use the Lax-Friedrichs (LF) flux: $h(a,b) = \frac{1}{2}[f(a)+f(b)-\beta(b-a)]$, where $\beta = \max_u |f'(u)|$ is the largest characteristic speed. For systems of conservation laws, we use a component-wise extension of (3.1) without characteristic decomposition.

3.1. A 5th Order Central Reconstruction in 1D.

Assume the approximate cell average $\overline{U}_i$ is given at cell C_i, with cell center x_i, $i = 1, 2, \cdots, 5$, see figure 2 left. In order to construct a 4th degree polynomial $U_3(x-x_3) = U_3(0)+U_3'(0)(x-x_3)+\frac{1}{2}U_3''(0)(x-x_3)^2+\frac{1}{3!}U_3^{(3)}(0)(x-x_3)^3+\frac{1}{4!}U_3^{(4)}(0)(x-x_3)^4$ in cell C_3, one solves the following linear system

$$\frac{1}{|C_i|}\int_{C_i} U_3(x-x_3)dx = \overline{U}_i, \quad i = 1,2,3,4,5.$$

The reconstructed polynomial can be oscillatory near discontinuities of the solution. The next step is to apply the hierarchical reconstruction to remove possible spurious oscillations.

3.2. A 4th Order Central Reconstructions in 2D.

In figure 5 left, in order to reconstruct a cubic polynomial in cell C_7, we use the similar method as in Sec. 2.2.2.

3.3. A 5th Order finite difference scheme in 2D.

In Shu and Osher [37], an efficient finite difference ENO scheme is developed for uniform rectangular grid in multi space dimensions. It only uses a 1D finite volume ENO reconstruction of a function from its 1D cell averages. These 1D cell averages are set to be equal to the point values of a flux function at the corresponding cell centers. Characteristic decomposition is necessary for higher order reconstructions, such as the fifth order ENO or WENO reconstruction, to avoid spurious oscillations. Here we use the finite difference framework of [37] and combine it with the 1D fifth order central finite volume reconstruction in Sec.3.1 followed by the 1D hierarchical reconstruction (see Sec. 4). This modified finite difference scheme is implemented without characteristic decomposition.

4. Non-Oscillatory Hierarchical Reconstruction

The central reconstruction out of nearby cell averages generates a polynomial in each cell. However, the solution of nonlinear conservation laws may contain discontinuities, and the Gibbs phenomenon could appear in reconstructed polynomials. We are going to apply the non-oscillatory hierarchical reconstruction procedure developed in [28] to remove the possible oscillations and achieve higher resolution near discontinuities. This technique has been developed for the central discontinuous Galerkin formulation in [28]. We show that it also works for finite volume schemes with simple central reconstructions.

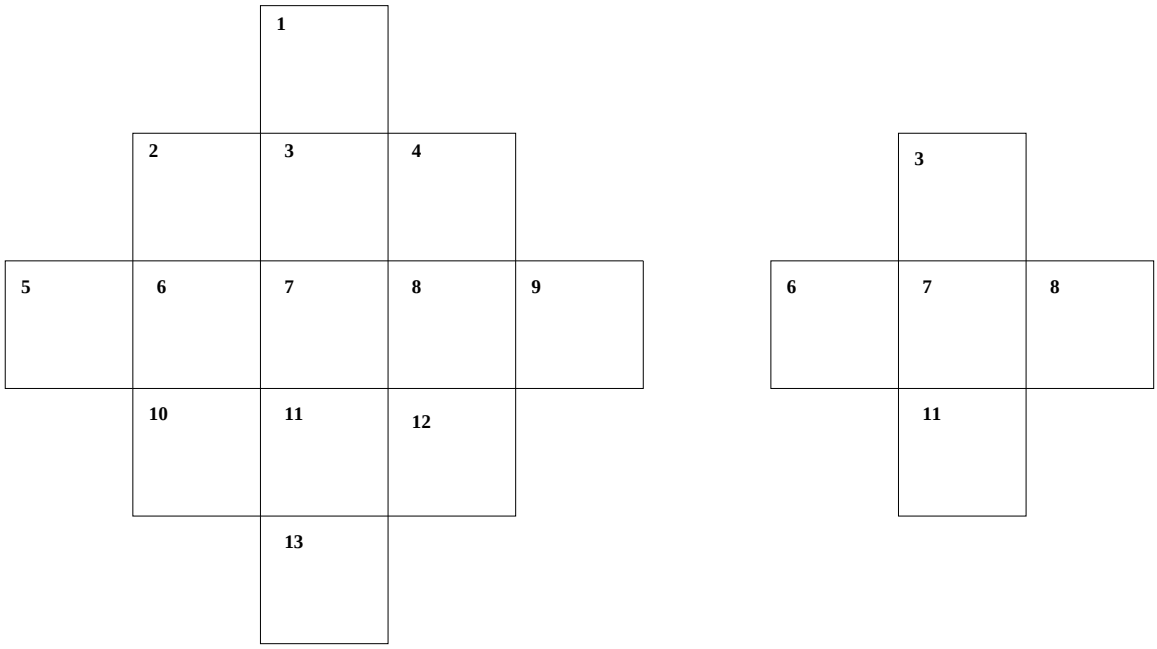

Figure 5: Left: a 4th order central finite volume reconstruction in cell 7 uses cell averages in cell $1, 2, \cdots, 13$. Right: the hierarchical reconstruction in cell 7 involves only polynomials in cell $3, 6, 7, 8, 11$.

From the central or finite volume schemes with the SSP Runge-Kutta time stepping methods, we obtain a piece-wise polynomial solution $U(\mathbf{x})$ (and $V(\mathbf{x})$ for dual cells in overlapping grids) at a Runge-Kutta stage, after applying central reconstructions. For example, for the uniform overlapping grid (see figure 1 for 2D case), we can write

$$U(\mathbf{x}) = \sum_{I+1/2} U_{I+1/2}(\mathbf{x} - \mathbf{x}_{I+1/2})\mathbf{1}_{C_{I+1/2}}(\mathbf{x}) \in \mathcal{M} \quad \text{and} \quad V(\mathbf{x}) = \sum_{I} V_I(\mathbf{x} - \mathbf{x}_I)\mathbf{1}_{D_I}(\mathbf{x}) \in \mathcal{N},$$

recalling that $\mathbf{x}_{I+1/2}$ and $\mathbf{x}_I$ are centroids of cell $C_{I+1/2}$ and D_I respectively; $U_{I+1/2}(\mathbf{x} - \mathbf{x}_{I+1/2})$ and $V_I(\mathbf{x} - \mathbf{x}_I)$ are the polynomials (of degree r) in cells $C_{I+1/2}$ and D_I respectively. The task is to reconstruct a 'limited' version of the polynomial in cell $C_{I+1/2}$, retaining high order accuracy and removing spurious oscillations. For convenience the adjacent cells are renamed as the set $\{C_J\}$ (which contain cell $C_{I+1/2}$, D_I *etc*), and the polynomials (of degree r) supported on them are thus renamed as $\{U_J(\mathbf{x} - \mathbf{x}_J)\}$ respectively, where $\mathbf{x}_J$ is the cell centroid of cell C_J. We write $U_{I+1/2}(\mathbf{x} - \mathbf{x}_{I+1/2})$ in terms of its Taylor expansion,

$$U_{I+1/2}(\mathbf{x} - \mathbf{x}_{I+1/2}) = \sum_{m=0}^{r} \sum_{|\mathbf{m}|=m} \frac{1}{\mathbf{m}!} U^{(\mathbf{m})}_{I+1/2}(\mathbf{0})(\mathbf{x} - \mathbf{x}_{I+1/2})^{\mathbf{m}},$$

where $\dfrac{1}{\mathbf{m}!} U^{(\mathbf{m})}_{I+1/2}(\mathbf{0})$ are the coefficients which participate in its typical m-degree terms,

$$\sum_{|\mathbf{m}|=m} \frac{1}{\mathbf{m}!} U^{(\mathbf{m})}_{I+1/2}(\mathbf{0})(\mathbf{x} - \mathbf{x}_{I+1/2})^{\mathbf{m}}, \ |\mathbf{m}| = 0, \ldots, r.$$

In the following, we briefly describe the hierarchical reconstruction procedure to recompute the polynomial $U_{I+1/2}(\mathbf{x} - \mathbf{x}_{I+1/2})$ by using polynomials in cells $\{C_J\}$. It describes a procedure to compute

the new coefficients

$$\frac{1}{\mathbf{m}!}\widetilde{U}^{(\mathbf{m})}_{I+1/2}(\mathbf{0}), \qquad m = r, r-1, \ldots, 0$$

in $U_{I+1/2}(\mathbf{x}-\mathbf{x}_{I+1/2})$, iterating from the highest to the lowest degree terms.

To reconstruct $\widetilde{U}^{(\mathbf{m})}_{I+1/2}(\mathbf{0})$, we first compute many *candidates* of $U^{(\mathbf{m})}_{I+1/2}(\mathbf{0})$ (sometimes still denoted as $\widetilde{U}^{(\mathbf{m})}_{I+1/2}(\mathbf{0})$ with specification), and we then let the new coefficient for $U^{(\mathbf{m})}_{I+1/2}(\mathbf{0})$ be

$$\widetilde{U}^{(\mathbf{m})}_{I+1/2}(\mathbf{0}) = F\big(\text{ candidates of } U^{(\mathbf{m})}_{I+1/2}(\mathbf{0})\ \big),$$

where F is a convex limiter of its arguments.

In order to find these candidates of $U^{(\mathbf{m})}_{I+1/2}(\mathbf{0})$, $|\mathbf{m}| = m$, we take a $(m-1)$-th order partial derivative of $U_{I+1/2}(\mathbf{x}-\mathbf{x}_{I+1/2})$, and denote it by

$$\partial^{m-1}U_{I+1/2}(\mathbf{x}-\mathbf{x}_{I+1/2}) = L_{I+1/2}(\mathbf{x}-\mathbf{x}_{I+1/2}) + R_{I+1/2}(\mathbf{x}-\mathbf{x}_{I+1/2}),$$

where $L_{I+1/2}$ is the linear part and $R_{I+1/2}$ is the remainder. Clearly, a 'candidate' for a coefficient in the first degree terms of $L_{I+1/2}$ is the candidate for the corresponding $U^{(\mathbf{m})}_{I+1/2}(\mathbf{0})$.

In order to find the candidates for all the coefficients in the first degree terms of $L_{I+1/2}(\mathbf{x}-\mathbf{x}_{I+1/2})$, we only need to know the *new approximate cell averages* of $L_{I+1/2}(\mathbf{x}-\mathbf{x}_{I+1/2})$ on $d+1$ distinct mesh cells adjacent to cell $C_{I+1/2}$, where d is the spatial dimension. The set of these $d+1$ cells with given new approximate cell averages is called a *stencil*.

Algorithm 1. Step 1. *Suppose $r \geq 2$. For $m = r, r-1, \cdots, 2$, do the following:*

(a) Take a $(m-1)$-th order partial derivative for each of $\{U_J(\mathbf{x}-\mathbf{x}_J)\}$ to obtain polynomials $\{\partial^{m-1}U_J(\mathbf{x}-\mathbf{x}_J)\}$ respectively. In particular, denote $\partial^{m-1}U_{I+1/2}(\mathbf{x}-\mathbf{x}_{I+1/2}) = L_{I+1/2}(\mathbf{x}-\mathbf{x}_{I+1/2}) + R_{I+1/2}(\mathbf{x}-\mathbf{x}_{I+1/2})$, where $L_{I+1/2}(\mathbf{x}-\mathbf{x}_{I+1/2})$ is the linear part of $\partial^{m-1}U_{I+1/2}(\mathbf{x}-\mathbf{x}_{I+1/2})$ and $R_{I+1/2}(\mathbf{x}-\mathbf{x}_{I+1/2})$ is the remainder.

(b) Calculate the cell averages of $\{\partial^{m-1}U_J(\mathbf{x}-\mathbf{x}_J)\}$ on cells $\{C_J\}$ to obtain $\{\overline{\partial^{m-1}U_J}\}$ respectively.

(c) Let $\widetilde{R}_{I+1/2}(\mathbf{x}-\mathbf{x}_{I+1/2})$ be the $R_{I+1/2}(\mathbf{x}-\mathbf{x}_{I+1/2})$ with its coefficients replaced by the corresponding new coefficients. Calculate the cell averages of $\widetilde{R}_{I+1/2}(\mathbf{x}-\mathbf{x}_{I+1/2})$ on cells $\{C_J\}$ to obtain $\{\overline{R}_J\}$ respectively.

(d) Let $\overline{L}_J = \overline{\partial^{m-1}U_J} - \overline{R}_J$ for all J.

(e) Form stencils out of the new approximate cell averages $\{\overline{L}_J\}$ by using a non-oscillatory finite volume MUSCL or second order ENO strategy. Each stencil will determine a set of candidates for the coefficients in the first degree terms of $L_{I+1/2}(\mathbf{x}-\mathbf{x}_{I+1/2})$, which are also candidates for the corresponding $U^{(\mathbf{m})}_{I+1/2}(\mathbf{0})$'s, $|\mathbf{m}| = m$.

(f) Repeat from (a) to (e) until all possible combinations of the $(m-1)$-th order partial derivatives are taken. Then the candidates for all coefficients in the m-th degree terms of $U_{I+1/2}(\mathbf{x}-\mathbf{x}_{I+1/2})$ have been computed. For each of these coefficients, say $\frac{1}{\mathbf{m}!}U^{(\mathbf{m})}_{I+1/2}(\mathbf{0})$, $|\mathbf{m}| = m$, let the new coefficient $\widetilde{U}^{(\mathbf{m})}_{I+1/2}(\mathbf{0}) = F\big(\text{ candidates of } U^{(\mathbf{m})}_{I+1/2}(\mathbf{0})\ \big)$, where F is a convex limiter.

Step 2. *In order to find the new coefficients in the zero-th and first degree terms of $U_{I+1/2}(\mathbf{x}-\mathbf{x}_{I+1/2})$, we perform the procedure of Step 1 (a)-(f) with $m = 1$, and make sure that the new approximate cell average $\overline{L}_{I+1/2}$ is in each of the stencils, which ensures that the cell average of $U_{I+1/2}(\mathbf{x}-\mathbf{x}_{I+1/2})$ on cell $C_{I+1/2}$ is not changed with new coefficients. The new coefficient in the zero-th degree term of $U_{I+1/2}(\mathbf{x}-\mathbf{x}_{I+1/2})$ is $\overline{L}_{I+1/2}$.*

It is shown in [28] the approximation order of accuracy of a polynomial in a cell is unaffected by the algorithm.

4.1. **An Example for 2D Overlapping Cells.** We briefly describe how to implement the hierarchical reconstruction for the piece-wise cubic polynomial reconstructed in Sec. 2.2.2. Suppose in cell C_j (see figure 3 right), a cubic polynomial is given as

$$\begin{aligned} U_j(x-x_j,y-y_j) &= U_j(0,0)+\partial_x U_j(0,0)(x-x_j)+\partial_y U_j(0,0)(y-y_j)+ \\ &\quad \frac{1}{2}\partial_{xx}U_j(0,0)(x-x_j)^2+\partial_{xy}U_j(0,0)(x-x_j)(y-y_j)+\frac{1}{2}\partial_{yy}U_j(0,0)(y-y_j)^2 \\ &\quad \frac{1}{6}\partial_{xxx}U_j(0,0)(x-x_j)^3+\frac{1}{2}\partial_{xxy}U_j(0,0)(x-x_j)^2(y-y_j)+ \\ &\quad \frac{1}{2}\partial_{xyy}U_j(0,0)(x-x_j)(y-y_j)^2+\frac{1}{6}\partial_{yyy}U_j(0,0)(y-y_j)^3, \end{aligned}$$

where (x_j,y_j) is the cell centroid of cell C_j, $j=4,5,7,9,10$.

According to Step 1 of Algorithm 1 with $m=3$, first take the $(m-1=2)$ 2nd order partial derivative ∂_{xx} for them to obtain $L_j(x-x_j,y-y_j)=\partial_{xx}U_j(0,0)+\partial_{xxx}U_j(0,0)(x-x_j)+\partial_{xxy}U_j(0,0)(y-y_j)$, $j=4,5,7,9,10$. Calculate the cell average of $L_j(x-x_j,y-y_j)$ on cell C_j to obtain $\overline{L}_j=\partial_{xx}U_j(0,0)$, $j=4,5,7,9,10$ (note that $R_7(x-x_7,y-y_7)\equiv 0$). With the five new approximate cell averages $\{\overline{L}_j : j=4,5,7,9,10\}$, one can apply a MUSCL or a second order ENO procedure to reconstruct a non-oscillatory linear polynomial

$$\widetilde{L}_7(x-x_7,y-y_7)=\partial_{xx}\widetilde{U}_7(0,0)+\partial_{xxx}\widetilde{U}_7(0,0)(x-x_7)+\partial_{xxy}\widetilde{U}_7(0,0)(y-y_7)$$

in cell C_7. In fact, we form four stencils $\{C_7,C_4,C_5\}$, $\{C_7,C_5,C_{10}\}$, $\{C_7,C_{10},C_9\}$ and $\{C_7,C_9,C_4\}$. For the first stencil, solve the following equations for $\partial_{xxx}\widetilde{U}_7(0,0)$ and $\partial_{xxy}\widetilde{U}_7(0,0)$

$$\begin{aligned} \frac{1}{|C_j|}\int_{C_j}\widetilde{L}_7(x-x_7,y-y_7)dxdy &= \overline{L}_7+\partial_{xxx}\widetilde{U}_7(0,0)(x_j-x_7)+\partial_{xxy}\widetilde{U}_7(0,0)(y_j-y_7) \\ &= \overline{L}_j, \end{aligned}$$

$j=4,5$, similarly for other stencils. We obtain two sets of candidates for $\partial_{xxx}U_7(0,0)$ and $\partial_{xxy}U_7(0,0)$ respectively. By taking the 2nd order partial derivative ∂_{xy} for $U_j(x-x_j,y-y_j)$, $j=4,5,7,9,10$, we similarly obtain a set of candidates for $\partial_{xyy}U_7(0,0)$ and enlarge the set of candidates for $\partial_{xxy}U_7(0,0)$. Taking the 2nd order partial derivative ∂_{yy} for $U_j(x-x_j,y-y_j)$, $j=4,5,7,9,10$, yields a set of candidates for $\partial_{yyy}U_7(0,0)$ and enlarge the set of candidates for $\partial_{xyy}U_7(0,0)$. Putting all candidates for $\partial_{xxx}U_7(0,0)$ into the arguments of a limiter function $F(\ )$, we obtain the new coefficient $\partial_{xxx}\widetilde{U}_7(0,0)$ for $\partial_{xxx}U_7(0,0)$. Applying the same procedure to obtain new coefficients $\partial_{xxy}\widetilde{U}_7(0,0)$, $\partial_{xyy}\widetilde{U}_7(0,0)$ and $\partial_{yyy}\widetilde{U}_7(0,0)$.

Repeat the above procedure with $m=2$. Note that the $R_7(x-x_7,y-y_7)$ term as defined in Algorithm 1 is non trivial now. For example, taking the 1st derivative ∂_x for $U_j(x-x_j,y-y_j)$, $j=4,5,7,9,10$, we obtain

$$\begin{aligned} \partial_x U_j(x-x_j,y-y_j) &= \partial_x U_j(0,0)+\partial_{xx}U_j(0,0)(x-x_j)+\partial_{xy}U_j(0,0)(y-y_j)+ \\ &\quad \frac{1}{2}\partial_{xxx}U_j(0,0)(x-x_j)^2+\partial_{xxy}U_j(0,0)(x-x_j)(y-y_j)+\frac{1}{2}\partial_{xyy}U_j(0,0)(y-y_j)^2 \\ &= L_j(x-x_j,y-y_j)+ \\ &\quad R_j(x-x_j,y-y_j), \quad j=4,5,7,9,10. \end{aligned}$$

We compute the cell average of $\partial_x U_j(x-x_j, y-y_j)$ on cell C_j to obtain $\overline{\partial_x U_j}$, $j = 4, 5, 7, 9, 10$; and compute cell averages of the polynomial

$$\widetilde{R}_7(x-x_7, y-y_7) = \frac{1}{2}\partial_{xxx}\widetilde{U}_7(0,0)(x-x_7)^2 + \partial_{xxy}\widetilde{U}_7(0,0)(x-x_7)(y-y_7) + \frac{1}{2}\partial_{xyy}\widetilde{U}_7(0,0)(y-y_7)^2$$

on cell C_j to obtain $\overline{R}_j$, $j = 4, 5, 7, 9, 10$. Redefine $\overline{L}_j = \overline{\partial_x U_j} - \overline{R}_j$, $j = 4, 5, 7, 9, 10$. The same MUSCL or second order ENO procedure as described previously can be applied to the five cell averages $\{\overline{L}_j : j = 4, 5, 7, 9, 10\}$ to obtain new coefficients for the first degree terms of $L_7(x-x_7, y-y_7)$, namely $\partial_{xx}\widetilde{U}_7(0,0)$ and $\partial_{xy}\widetilde{U}_7(0,0)$. Then we will take the 1st derivative ∂_y for $U_j(x-x_j, y-y_j)$, $j = 4, 5, 7, 9, 10$, and so on as described in Algorithm 1.

Remark. For the 2D non-staggered mesh, the stencils we use are similar, see figure 5 right. One dimensional hierarchical reconstruction in a cell only involves one adjacent cell on the left and one on the right, regardless the degree of polynomials, see figure 6.

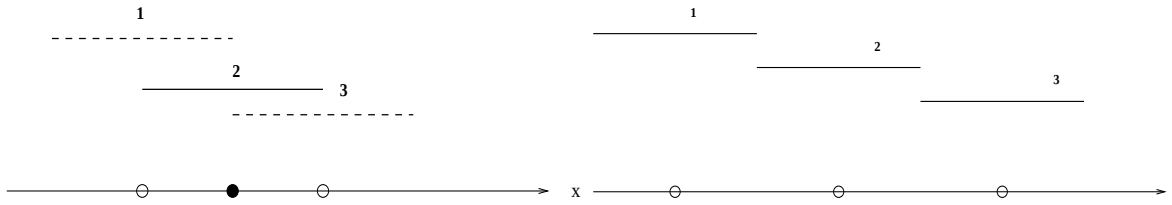

Figure 6: Left: 1D overlapping cells. Right: 1D non-staggered cells. Non-oscillatory hierarchical reconstruction for cell 2 involves only cells 1, 2 and 3.

4.2. **Remarks on Undershoots.** With the hierarchical reconstruction, there could still be some small overshoots or undershoots near discontinuities. For strong shocks, the undershoots could introduce non physical states. We find that in the computation of the double Mach reflection problem ([41], see Sec. 5), the non staggered finite volume schemes (Sec. 3) with the hierarchical reconstruction could introduce negative pressure at the shock front, where the pressure ratio across the shock is above 100. We set a lower bound p_{low} for the pressure, e.g., $p_{\text{low}} = \frac{3}{4}p_{\min}$ where $p_{\min}$ is the estimated lowest pressure ever occurred for the problem. At each time stage of the computation, if the pressure in a cell is below p_{low}, we redo the hierarchical reconstruction for the cell and its adjacent cells with the new coefficients for the polynomial terms of degrees above one set to be zero in Algorithm 1, and recompute the affected cell averages. This reduces the local formal accuracy to second order in possible trouble regions.

4.3. **Remarks on Limiters.** In [28], the convex limiter function $F(\,)$ used in the hierarchical reconstruction can be the minmod limiter

$$\text{minmod}\{c_1, c_2, \cdots, c_m\} = \begin{cases} \min\{c_1, c_2, \cdots, c_m\}, & \text{if } c_1, c_2, \cdots, c_m > 0, \\ \max\{c_1, c_2, \cdots, c_m\}, & \text{if } c_1, c_2, \cdots, c_m < 0, \\ 0, & \text{otherwise,} \end{cases} \tag{4.1}$$

so that the linear reconstruction at each stage is a MUSCL reconstruction; or it can be

$$\text{minmod}_2\{c_1, c_2, \cdots, c_m\} = c_j, \ \text{ if } |c_j| = \min\{|c_1|, |c_2|, \cdots, |c_m|\} \tag{4.2}$$

so that linear reconstruction at each stage is a second order ENO reconstruction. In certain situations these limiters used in the hierarchical reconstruction could degenerate the accuracy for approximating smooth solutions. This is due to the abrupt shift of stencils which reduces the smoothness of the

Δx	1/10	1/20	1/40	1/80	1/160
l_1 *error*	0.000138	4.42e-06	1.66e-07	6.77e-09	3.09e-10
order	-	4.96	4.73	4.62	4.45
l_∞ *error*	0.000201	8.95e-06	4.11e-07	2.33e-08	1.92e-09
order	-	4.49	4.44	4.14	3.60

TABLE 1. 5th order finite volume (Sec.3.1, 4 and (4.1)) for the 1D Burgers' equation.

Δx	1/10	1/20	1/40	1/80	1/160
l_1 *error*	1.24e-05	3.81e-07	1.21e-08	3.76e-10	1.18e-11
order	-	5.04	4.98	5.01	4.99
l_∞ *error*	2.16e-05	7.21e-07	3.28e-08	1.29e-09	5.62e-11
order	-	4.90	4.46	4.67	4.52

TABLE 2. 5th order central (Sec.2.2.1, 4 and (4.2)) for the 1D Burgers' equation.

Δx	1/4	1/8	1/16	1/32	1/64
l_1 *error*	8.21E-2	1.27E-2	1.60E-3	1.97E-4	2.43E-5
order	-	2.69	2.99	3.02	3.02
l_∞ *error*	5.10E-2	9.27E-3	1.62E-3	2.02E-4	2.86E-5
order	-	2.46	2.52	3.00	2.82

TABLE 3. 3rd order central (Sec.2.2.3, 4 and (4.2)) for the 2D Burgers' equation.

numerical flux. Following [35, 33], we can perturb the limiters slightly so that they become center biased. Define

$$\text{minmod}_{1.1}\{c_1, c_2, \cdots, c_m\} = \text{minmod}\left\{(1+\epsilon)\text{minmod}\{c_1, c_2, \cdots, c_m\}, \frac{1}{m}\sum_{i=1}^{m} c_i\right\}, \tag{4.3}$$

where ϵ is a small positive number. It is easy to see that $\text{minmod}_{1.1}$ still returns a convex combination of its arguments, and if $\epsilon = 0$, it becomes the minmod limiter. For all numerical experiments conducted in the paper, we take $\epsilon = 0.01$ and find that it does not increase the overshoots or undershoots at discontinuities significantly, and it slightly improves the resolution of the smooth solution near discontinuities.

4.4. **Remarks on the Complexity.** In the 2D code we have developed for the 4th order central scheme on overlapping cells (Sec.2.2.2) with the hierarchical reconstruction, we find that the hierarchical reconstruction takes about half of the total CPU time. Therefore, using a smoothness detector to turn off the hierarchical reconstruction in smooth regions will effectively reduce the overall complexity. Here we use the low cost smoothness detector in [7]. After the high degree (of degree r) polynomial solution is obtained in each cell by a central reconstruction, the jump of the solution at the center of each cell edge is measured for non-staggered meshes. If the jumps at the edges of a cell are smaller than $\Delta x^{(r+1)/2}$, the cell is considered to be in the smooth region and the hierarchical reconstruction will not be performed in the cell; otherwise hierarchical reconstruction will be performed in the cell. For staggered meshes, we only measure the jump at the cluster point of a cell where adjacent overlapping cells join. This smoothness detector is used for all 2D computations (except for accuracy tests for smooth solutions).

Δx	1/4	1/8	1/16	1/32	1/64
l_1 *error*	2.83E-2	2.72E-3	1.85E-4	1.16E-5	7.12E-7
order	-	3.38	3.88	4.00	4.03
l_∞ *error*	2.27E-2	2.32E-3	2.12E-4	1.43E-5	8.57E-7
order	-	3.29	3.45	3.89	4.06

TABLE 4. 4th order central (Sec.2.2.2) for the 2D Burgers' equation.

Δx	1/4	1/8	1/16	1/32	1/64
l_1 *error*	6.02E-2	5.91E-3	3.83E-4	2.19E-5	1.44E-6
order	-	3.35	3.95	4.13	3.93
l_∞ *error*	3.85E-2	4.24E-3	3.24E-4	2.38E-5	1.67E-6
order	-	3.18	3.71	3.77	3.83

TABLE 5. 4th order central (Sec.2.2.2, 4 and (4.2)) for the 2D Burgers' equation.

Δx	1/4	1/8	1/16	1/32	1/64
l_1 *error*	6.34E-2	5.93E-3	3.07E-4	1.35E-5	7.35E-7
order	-	3.42	4.27	4.51	4.20
l_∞ *error*	4.25E-2	4.66E-3	2.54E-4	1.63E-5	1.27E-6
order	-	3.19	4.20	3.96	3.68

TABLE 6. 4th order finite volume scheme (Sec.3.2, 4 and (4.3)) for the 2D Burgers' equation.

Δx	1/4	1/8	1/16	1/32	1/64
l_1 *error*	7.42E-2	4.22E-3	5.95E-05	2.40E-6	4.26E-8
order	-	4.13	6.15	4.63	5.82
l_∞ *error*	4.14E-2	4.63E-3	1.17E-4	5.45E-6	1.68E-7
order	-	3.16	5.31	4.42	5.02

TABLE 7. 5th order finite difference (Sec.3.3, 4 and (4.3)) for the 2D Burgers' equation.

5. Numerical Examples

In the numerical experiments, the third order TVD Runge-Kutta time discretization method [37] is applied to all schemes. When overlapping cells are used, only the solution in one class of the overlapping cells is shown in the graphs throughout this section. For systems of equations, the component-wise extensions of the scalar schemes (without characteristic decomposition) are used in all computations.

Example 1. The Burgers' equation $u_t + (\frac{1}{2}u^2)_x = 0$, $u(x,0) = \frac{1}{4} + \frac{1}{2}\sin(\pi x)$ with periodic boundary conditions. The errors are shown at the final time $T = 0.1$ when the solution is still smooth. The errors computed by the 5th order central scheme with hierarchical reconstruction (Sec.2.2.1, 4 and (4.2)) are listed in Table 2, with $\Delta\tau^n = \Delta x/1.5$, $\theta = 1/2$, $\Delta t^n = \min\{\theta * \Delta\tau^n, \Delta x^{5/3}\}$. The errors computed by the 5th order finite volume scheme with hierarchical reconstruction (Sec.3.1, 4 and (4.1)) are listed in Table 1, with $\Delta t^n = \min\{CFL * \Delta x/0.75, \Delta x^{5/3}\}$, $CFL = 0.9$.

Example 2. The 2D Burgers' equation with periodic boundary conditions: $u_t + (\frac{1}{2}u^2)_x + (\frac{1}{2}u^2)_y = 0$, $u(x,0) = \frac{1}{4} + \frac{1}{2}\sin(\pi(x+y))$. The errors are shown at the final time $T = 0.1$ when the solution is still

h	1/4	1/8	1/16	1/32	1/64
l_1 *error*	5.84E-5	3.77E-6	2.36E-7	1.55E-8	1.26E-9
order	-	3.95	4.00	3.93	3.62
l_∞ *error*	2.15E-4	2.50E-5	2.63E-6	3.12E-7	3.54E-8
order	-	3.10	3.25	3.08	3.14

TABLE 8. 4th order central (Sec.2.2.2, 4 and (4.3)) on an irregular overlapping mesh (such that for one class of cells, $\Delta x = \Delta y = h$ in the upper half domain and $\Delta x = 2\Delta y = h$ in the lower half domain) for the 2D Euler equation.

smooth. The errors computed by the 3rd order central (Sec.2.2.3, 4 and (4.2)) are listed in Table 3, with $\Delta\tau^n$ determined with CFL number 0.4, $\theta = 0.9$. The errors computed by the 4th order central scheme without hierarchical reconstruction (Sec.2.2.2) are listed in Table 4, with $\Delta\tau^n$ determined with CFL number 0.4, $\Delta t^n = \min\{0.9 * \Delta\tau^n, \Delta x^{4/3}\}$. The errors with hierarchical reconstruction (Sec.2.2.2, 4 and (4.2)) are listed in Table 5. The errors computed by the 4th order finite volume scheme (Sec.3.2, 4 and (4.3)) are listed in Table 6, with Δt^n determined by CFL factor 0.5 or equal to $\Delta x^{4/3}$, whichever is smaller. The errors computed by the 5th order finite difference scheme (Sec.3.3, 4 and (4.3)) are listed in Table 7, with Δt^n determined by CFL factor 0.4 or equal to $\Delta x^{5/3}$, whichever is smaller.

Example 3. The 2D Euler equation can written as

$$\mathbf{u}_t + \mathbf{f}(\mathbf{u})_x + \mathbf{g}(\mathbf{u})_y = 0,\ \mathbf{u} = (\rho, \rho u, \rho v, E)^T,\ p = (\gamma - 1)(E - \tfrac{1}{2}\rho(u^2 + v^2))$$
$$\mathbf{f}(\mathbf{u}) = (\rho u, \rho u^2 + p, \rho uv, u(E + p))^T,\ \mathbf{g}(\mathbf{u}) = (\rho v, \rho uv, \rho v^2 + p, v(E + p))^T,$$

where $\gamma = 1.4$. There is a set of exact solution (and thus the initial value) given by $\rho = 1 + 0.5 * \sin(x + y - (u + v)t)$, $u = 1$, $v = -0.7$ and $p = 1$. We conduct a convergence test for the 4th order central scheme (Sec.2.2.2, 4 and (4.3)) on an irregular mesh on the spatial domain $[0, 1] \times [0, 1]$, from time $t = 0$ to $t = 0.1$. The irregular staggered mesh is such that for one class of the overlapping cells, the cell size is $\Delta x = \Delta y = h$ in the upper half domain and is $\Delta x = 2\Delta y = h$ in the lower half domain. The density errors are shown at the final time in Table 8.

Example 4. We compute the 1D Euler equation with Lax's initial data. $u_t + f(u)_x = 0$ with $u = (\rho, \rho v, E)^T$, $f(u) = (\rho v, \rho v^2 + p, v(E + p))^T$, $p = (\gamma - 1)(E - \frac{1}{2}\rho v^2)$, $\gamma = 1.4$. Initially, the density ρ, momentum ρv and total energy E are 0.445, 0.311 and 8.928 in $(0, 0.5)$; 0.5, 0 and 1.4275 in $(0.5, 1)$. The computed density profiles by various numerical schemes with hierarchical reconstruction are shown at $T = 0.16$ in figure 7 with $\Delta x = 1/200$. For central schemes on overlapping cells, $\Delta\tau^n$ is chosen with CFL factor 0.4, $\Delta t^n = 0.5\Delta\tau^n$. For finite volume schemes, Δt^n is determined with CFL factor 0.9.

Example 5. Shu-Osher problem [38]. It is the Euler equation with initial data

$$\begin{aligned}(\rho, v, p) &= (3.857143,\ 2.629369,\ 10.333333), \quad \text{for } x < -4,\\ (\rho, v, p) &= (1 + 0.2\sin(5x),\ 0,\ 1), \quad \text{for } x \geq -4.\end{aligned}$$

The density profiles computed by various numerical schemes with hierarchical reconstruction are plotted at $T = 1.8$, with $\Delta x = 1/40$ by default, see figure 8. For central schemes on overlapping cells, $\Delta\tau^n$ is chosen with CFL factor 0.5, $\Delta t^n = 0.5\Delta\tau^n$. For finite volume schemes, Δt^n is determined with CFL factor 0.9.

Example 6. Woodward and Colella problem [41] for the Euler equation computed by various numerical schemes with hierarchical reconstruction. Initially, the density, momentum, total energy are $1, 0, 2500$ in $(0, 0.1)$; $1, 0, 0.025$ in $(0.1, 0.9)$; $1, 0, 250$ in $(0.9, 1)$. For central schemes on overlapping

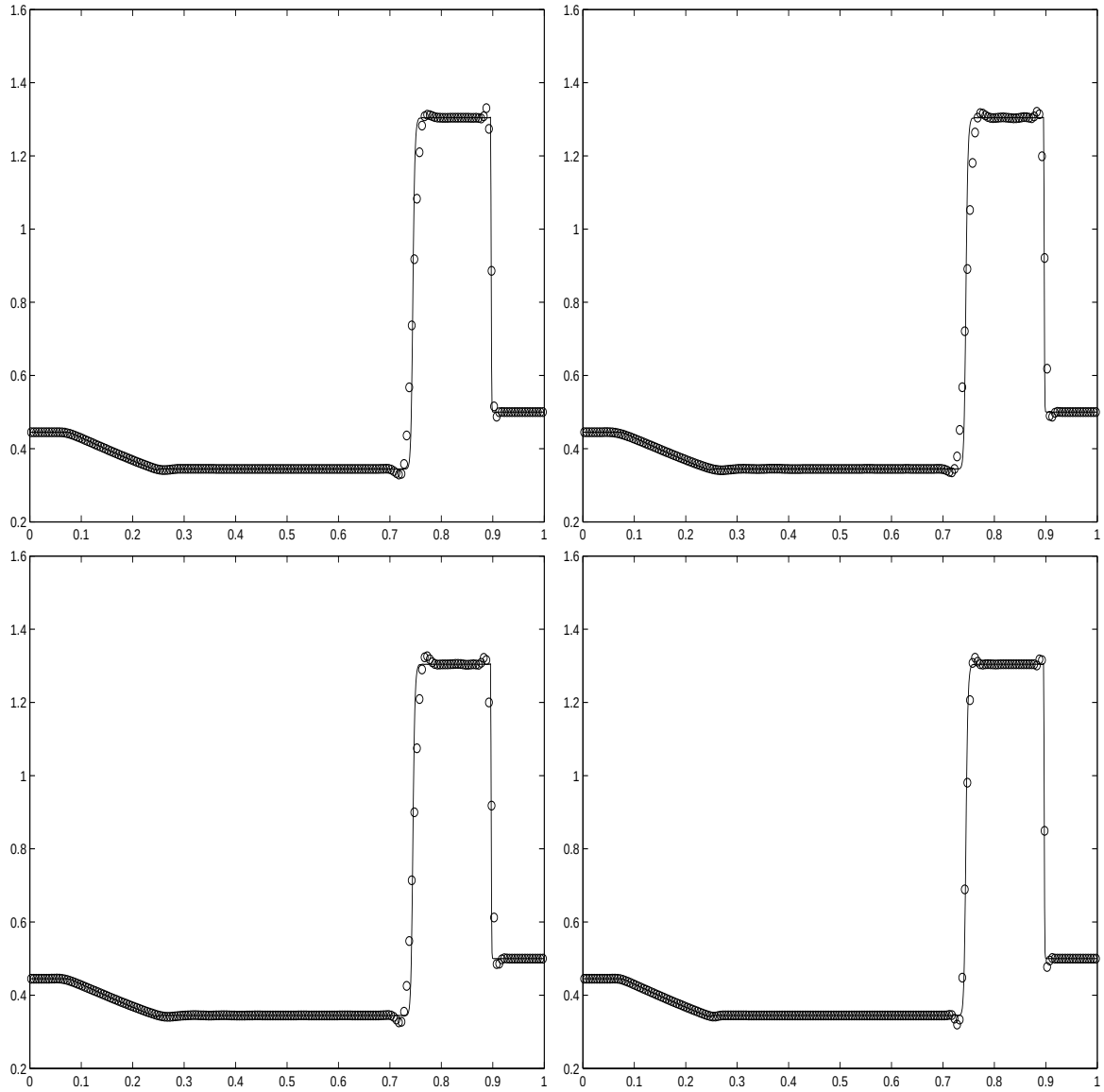

Figure 7: Comparative results of density for Lax's Problem, $\Delta x = 1/200$. From left to right, top to bottom. (1) 3rd order central (Sec.2.2.3, 4 and (4.2)); (2) 5th order finite volume scheme (Sec.3.1, 4 and (4.1)); (3) 5th order finite volume scheme (Sec.3.1, 4 and (4.3)); (4) 5th order central scheme (Sec.2.2.1, 4 and (4.2)).

cells, $\Delta\tau^n$ is chosen with CFL factor 0.4, $\Delta t^n = 0.5\Delta\tau^n$. For finite volume schemes, Δt^n is determined with CFL factor 0.5. Comparison of density profiles at $T = 0.01$ and $T = 0.038$ of different schemes with hierarchical reconstruction can be found in figure 9.

Example 7. Double Mach reflection [41] computed by various numerical schemes with hierarchical reconstruction. A planar Mach 10 shock is incident on an oblique wedge at a $\pi/3$ angle. The air in front of the shock has density 1.4, pressure 1 and velocity 0. It is described by the 2D Euler equation with $\gamma = 1.4$, and the boundary condition is described in [41]. The density profiles are plotted at $T = 0.2$ in figure 10 and 11, with 30 equally spaced contours. For central schemes on overlapping cells, $\Delta\tau^n$ is chosen with CFL factor 0.45; for finite volume schemes, Δt^n is determined with CFL factor 0.5; for the

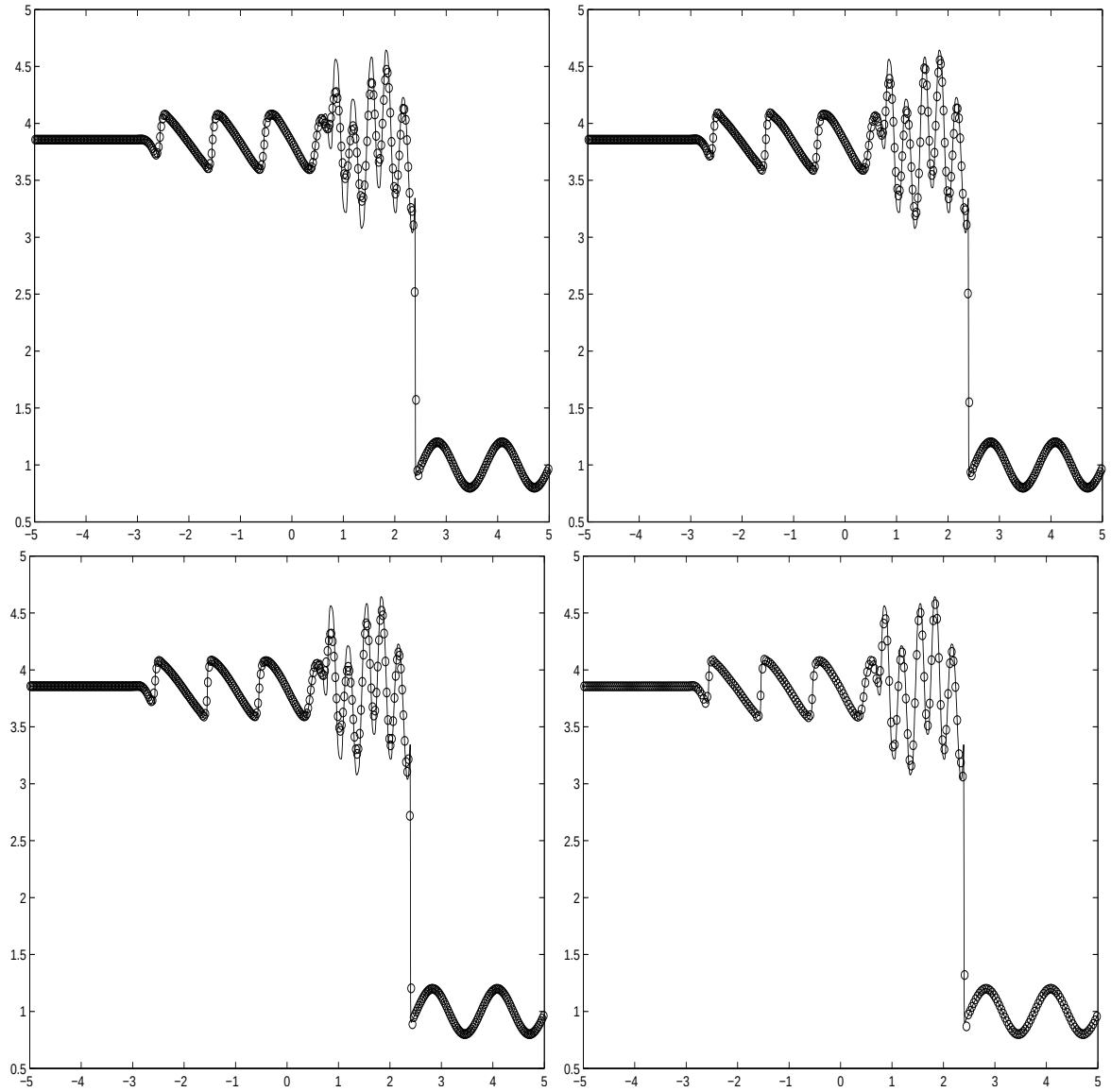

Figure 8: Shu-Osher Problem, $\Delta x = 1/40$ by default. From left to right, top to bottom, (1) 5th order finite volume scheme (Sec.3.1, 4 and (4.1)); (2) 5th order finite volume scheme (Sec.3.1, 4 and (4.3)); (3) 3rd order central (Sec.2.2.3, 4 and (4.2)); (4) 5th order central scheme (Sec.2.2.1, 4 and (4.1)), $\Delta x = 1/28$.

5th order finite difference (Sec.3.3, 4 and (4.3)), Δt^n is determined with CFL factor 0.4. The density along the line $y = 1/3$ is plotted against x in figure 12, on a mesh with $\Delta x = \Delta y = 1/120$. We can see that computed results are non-oscillatory on this mesh. In figure 13, we show the density contour computed by the 5th order finite difference (Sec.3.3, 4 and (4.3)) on a mesh with $\Delta x = \Delta y = 1/960$. In figure 14, the 4th order central (Sec.2.2.2, 4 and (4.2)) is applied to an irregular mesh such that for one class of cells, $\Delta x = \Delta y = h$ in the upper half domain and $\Delta x = 2\Delta y = h$ in the lower half domain. We can see in the graph that across the border line $y = 0.5$ separating two different grids, the horizontal shock becomes thicker while the vertical shock is almost unchanged.

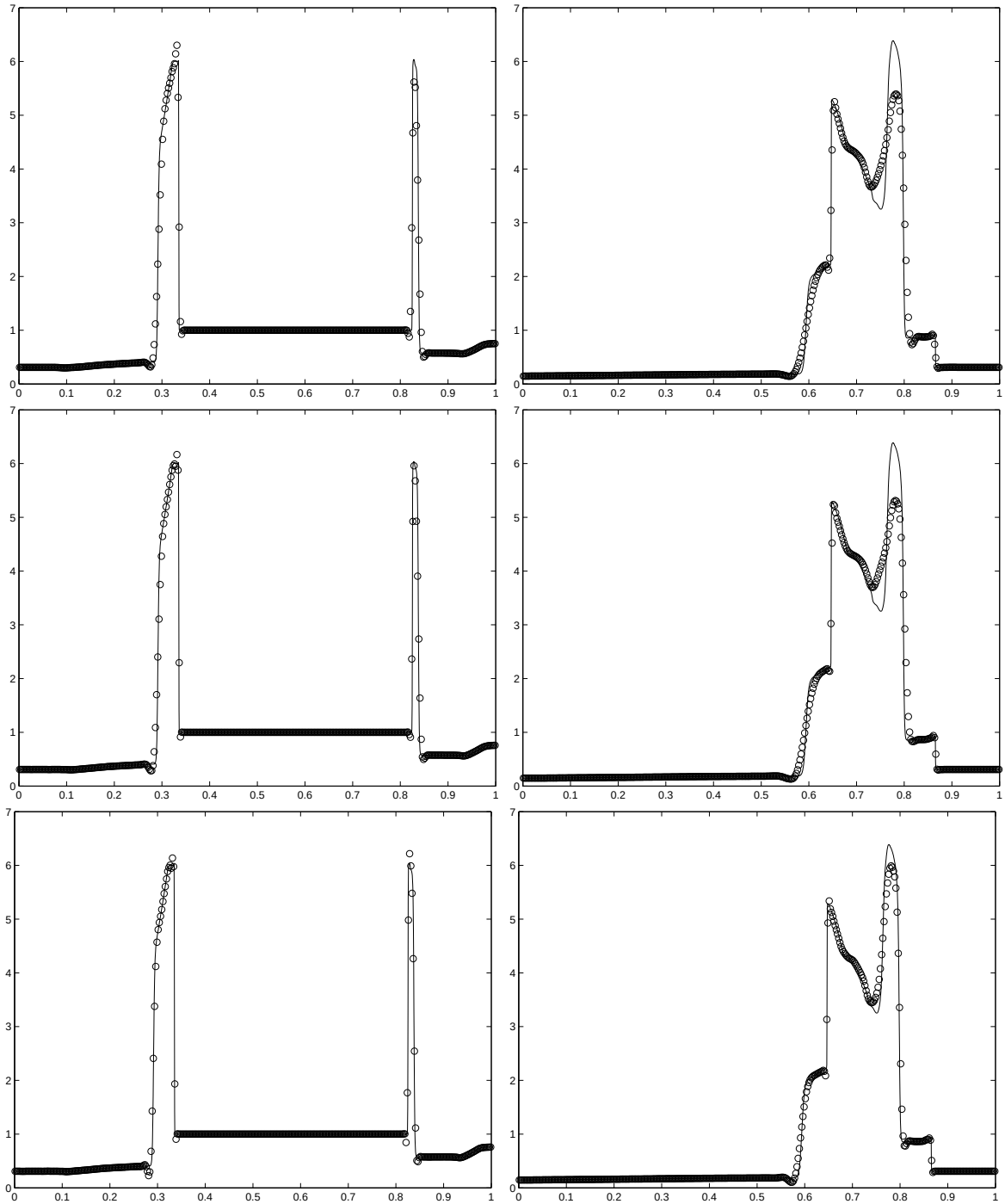

Figure 9: Woodward and Colella Problem. Comparison of density profiles at $T = 0.01$ (left) and $T = 0.038$ (right). $\Delta x = 1/400$. The 1st row: 5th order finite volume scheme (Sec.3.1, 4 and (4.3)); 2nd row: 3rd order central (Sec.2.2.3, 4 and (4.2)); 3rd row: 5th order central (Sec.2.2.1, 4 and (4.2)).

Example 8. 2D Riemann problem [23] for the Euler equation. The computational domain is $[0, 1] \times [0, 1]$. The initial states are constants within each of the 4 quadrants. Counter-clock-wisely from the

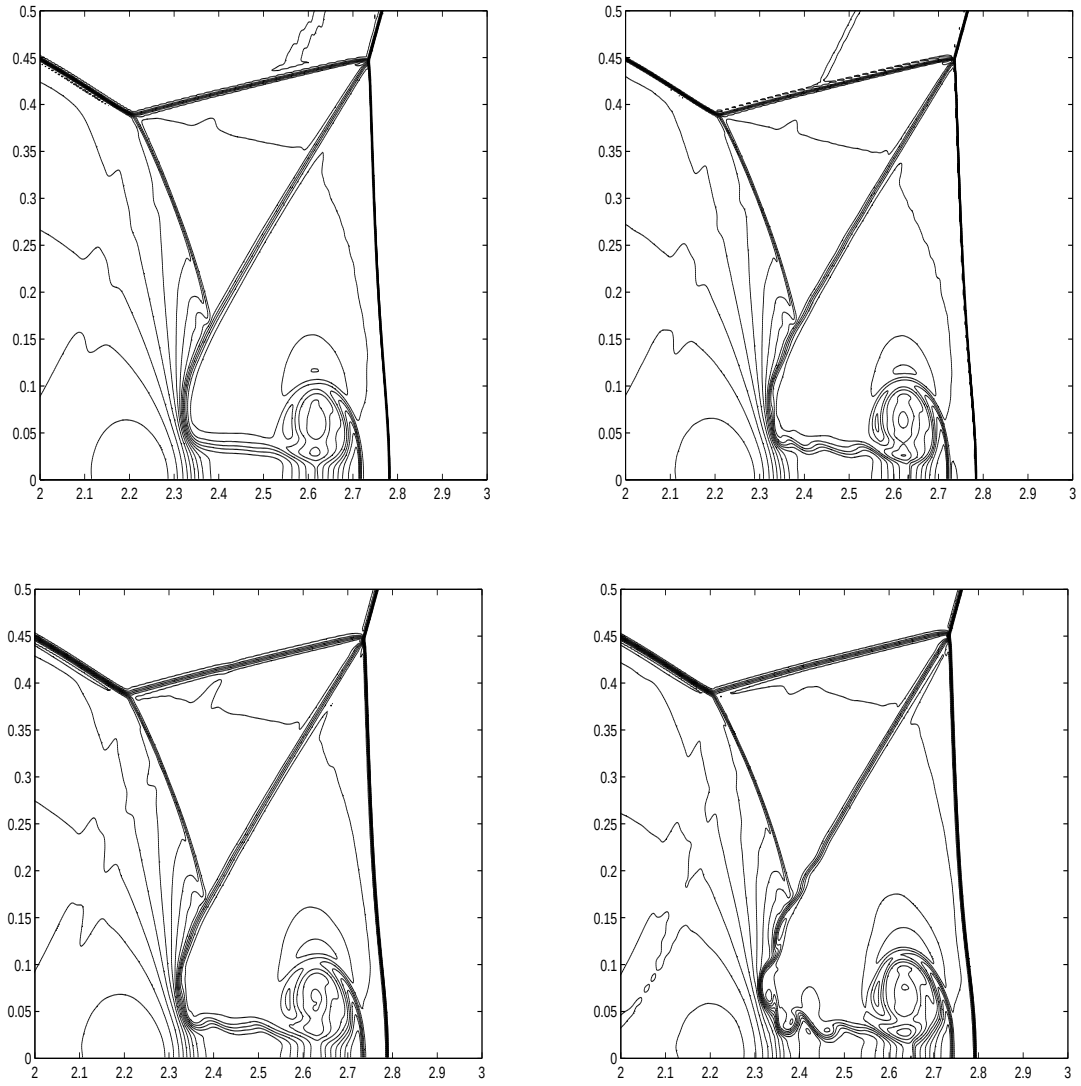

Figure 10: Density contours of the double Mach reflection, $\Delta x = \Delta y = 1/480$. From top to bottom, left to right: (1) 3rd order central (Sec.2.2.3, 4 and (4.2)); (2) 4th order central (Sec.2.2.2, 4 and (4.2)); (3) 4th order finite volume (Sec.3.2, 4 and (4.3)); (4) 5th order finite difference (Sec.3.3, 4 and (4.3)).

upper right quadrant, they are labeled as (ρ_i, u_i, v_i, p_i), $i = 1, 2, 3, 4$. Initially, $\rho_1 = 1.1$, $u_1 = 0$, $v_1 = 0$, $p_1 = 1.1$; $\rho_2 = 0.5065$, $u_2 = 0.8939$, $v_2 = 0$, $p_2 = 0.35$; $\rho_3 = 1.1$, $u_3 = 0.8939$, $v_3 = 0.8939$, $p_3 = 1.1$; $\rho_4 = 0.5065$, $u_4 = 0$, $v_4 = 0.8939$, $p_4 = 0.35$. We want to further check two schemes for the problem: the 4th order central scheme on irregular overlapping cells and the 5th order finite difference scheme, both with hierarchical reconstruction. The density contours are plotted at $T = 0.25$ in figure 15, with 40 equally spaced contours. The density profiles along $x = 0.8$ are plotted in figure 16. We can see that the solutions of these high order schemes are not oscillatory from these graphs. It should be noticed that lower order schemes can perform just as well for this problem, see e.g. [23, 22].

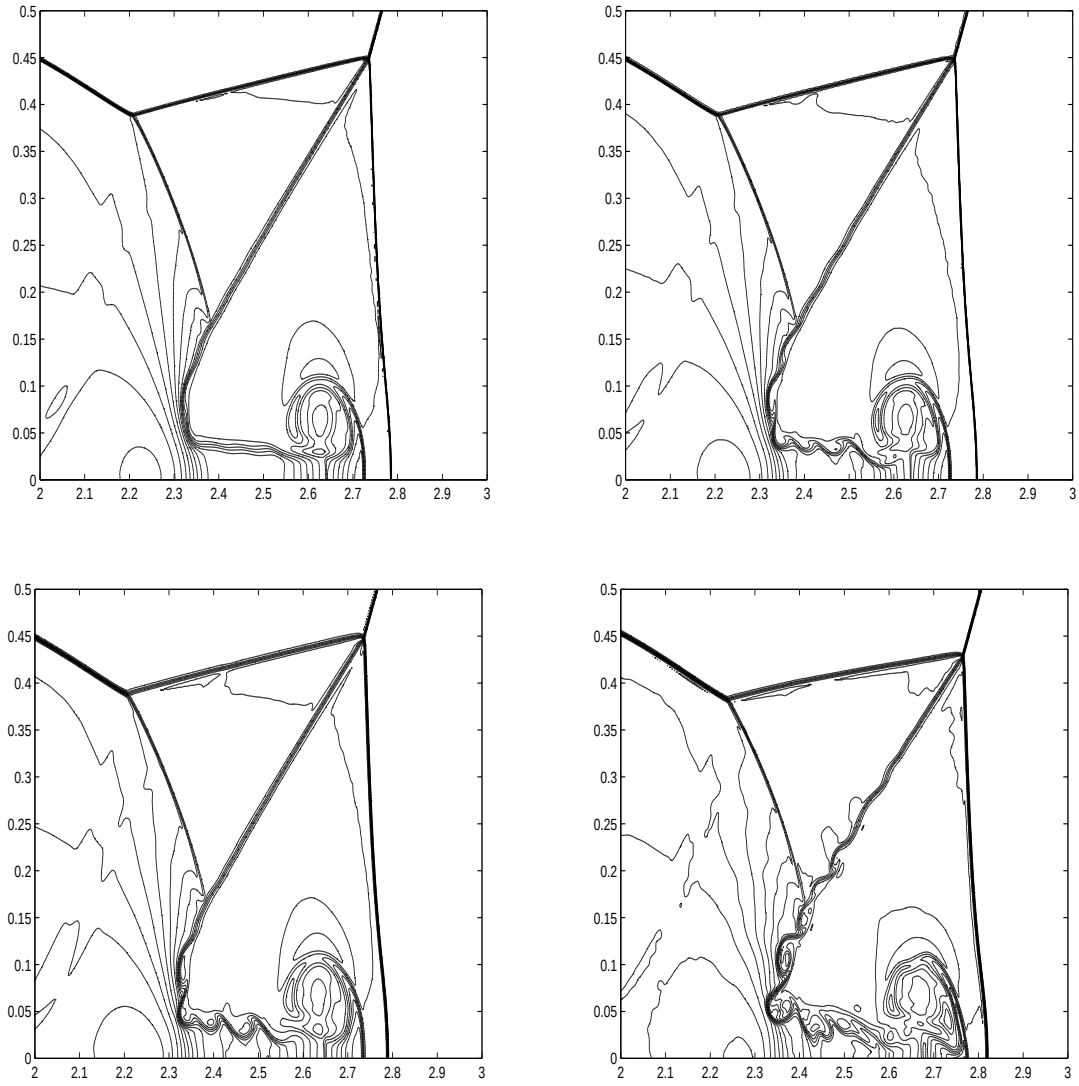

Figure 11: Density contours of the double Mach reflection, $\Delta x = \Delta y = 1/600$ by default. From top to bottom, left to right: (1) 3rd order central (Sec.2.2.3, 4 and (4.2)), $\Delta x = \Delta y = 1/720$; (2) 4th order central (Sec.2.2.2, 4 and (4.2)); (3) 4th order finite volume scheme (Sec.3.2, 4 and (4.3)); (4) 5th order finite difference (Sec.3.3, 4 and (4.3)).

5.1. **Remarks on Numerical Experiments.** The CPU time on an AMD Athlon 2ghz processor for the computation of the double Mach reflection (Example 7) on a mesh with $\Delta x = \Delta y = 1/120$ is 18 minutes for the 5th order finite difference (Sec.3.3, 4 and (4.3)); 47 minutes for the 4th order finite volume scheme (Sec.3.2, 4 and (4.3)); 38 minutes for the 3rd order central on overlapping cells (Sec.2.2.3, 4 and (4.2)); 77 minutes for the 4th order central on overlapping cells (Sec.2.2.2, 4 and (4.2)). The codes are written in C++ and are compiled by "$g++ -O4$". The complexity data is highly subjective to the programming and compiler. Even though central schemes on overlapping cells are more expensive, from our experience they tend to be more robust without characteristic decomposition for higher order: having smaller overshoots/undershoots at discontinuities and smoother solutions

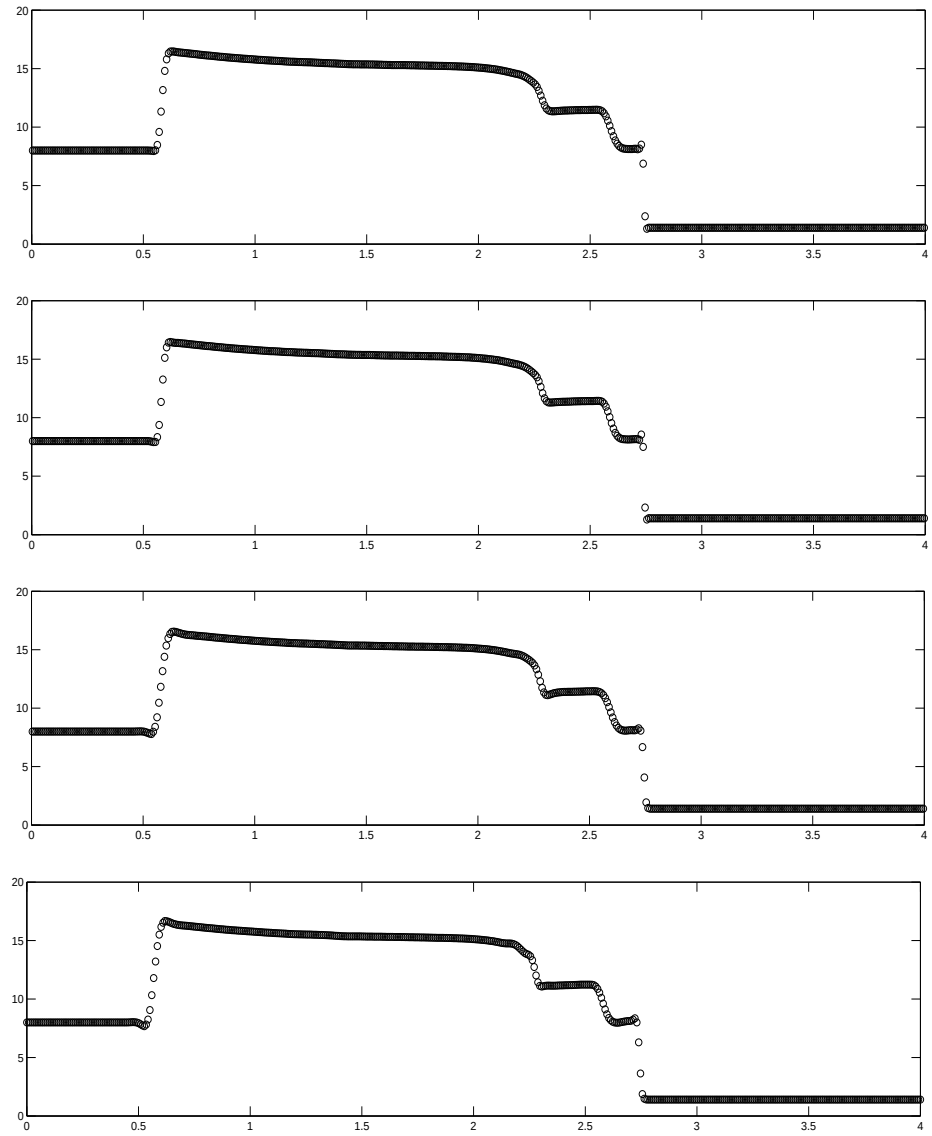

Figure 12: Double Mach reflection on a mesh with $\Delta x = \Delta y = 1/120$. Density plot along $y = 1/3$. From top to bottom: (1) 3rd order central (Sec.2.2.3, 4 and (4.2)); (2) 4th order central (Sec.2.2.2, 4 and (4.2)); (3) 4th order finite volume (Sec.3.2, 4 and (4.3)); (4) 5th order finite difference (Sec.3.3, 4 and (4.3)).

elsewhere (e.g., by comparing the constant solutions in $[0.7, 0.9]$ for the Lax problem, figure 7). For the non-staggered 4th and 5th order schemes we need to fix the negative pressure problem (due to the undershoots) for very strong shocks (Example 7).

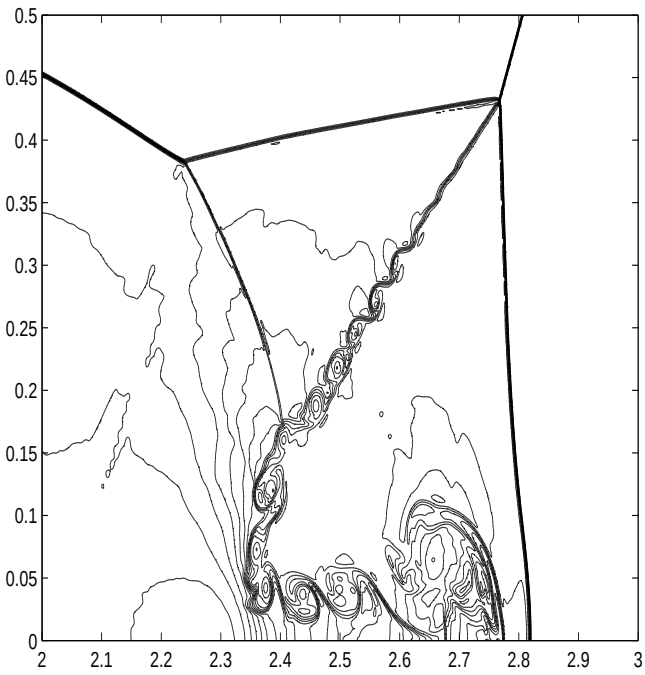

Figure 13: Density contour of the double Mach reflection on a mesh $\Delta x = \Delta y = 1/960$, computed by the 5th order finite difference (Sec.3.3, 4 and (4.3)).

References

[1] P. Arminjon and A. St-Cyr, *Nessyahu-Tadmor-type central finite volume methods without predictor for 3d cartesian and unstructured tetrahedral grids*, Appl. Numer. Math., 46 (2003), pp. 135–155.

[2] P. Arminjon, M. C. Viallon, A. Madrane, and L. Kaddouri, *Discontinuous finite elements and 2-dimensional finite volume versions of the Lax-Friedrichs and Nessyahu-Tadmor difference schemes for compressible flows on unstructured grids*, CFD Review, (M. Hafez and K. Oshima, Eds), John Wiley, (1997), pp. 241–261.

[3] T. Barth and P. Frederickson, *High order solution of the Euler equations on unstructured grids using quadratic reconstruction*, AIAA Paper No. 90-0013.

[4] F. Bianco, G. Puppo, and G. Russo, *High-order central schemes for hyperbolic systems of conservation laws*, SIAM J. Sci. Comput., 21 (1999), pp. 294–322.

[5] R. Biswas, K. Devine, and J. Flaherty, *Parallel, adaptive finite element methods for conservation laws*, Appl. Numer. Math., 14 (1994), pp. 255–283.

[6] J. Boris and D. Book, *Flux corrected transport I, SHASTA, a fluid transport algorithm that works*, J. Comput. Phys., 11 (1973), pp. 38–69.

[7] N. Chevaugeon, J. Xin, P. Hu, X. Li, D. Cler, J. Flaherty, and M. Shephard, *Discontinuous Galerkin methods applied to shock and blast problems*, J. Sci. Comput., 22/23 (2005), pp. 227–243.

[8] B. Cockburn and C.-W. Shu, *TVB Runge-Kutta local projection discontinuous Galerkin finite element method for conservation laws II, general framework*, Math. Comp., 52 (1989), pp. 411–435.

[9] ———, *The Runge-Kutta local projection p^1-discontinuous-Galerkin finite element method for scalar conservation laws*, RAIRO Model. Math. Anal. Numer., 25 (1991), pp. 337–361.

[10] ———, *The Runge-Kutta discontinuous Galerkin method for conservation laws V: multidimensional systems*, J. Comput. Phys., 141 (1998), pp. 199–224.

[11] P. Colella and P. Woodward, *The piecewise parabolic method (PPM) for gas-dynamical simulation*, J. Comput. Phys., 54 (1984), pp. 174–201.

[12] D. Gottlieb, C.-W. Shu, and E. Tadmor, *Strong stability-preserving high order time discretization methods*, SIAM Review, 43 (2001), pp. 89–112.

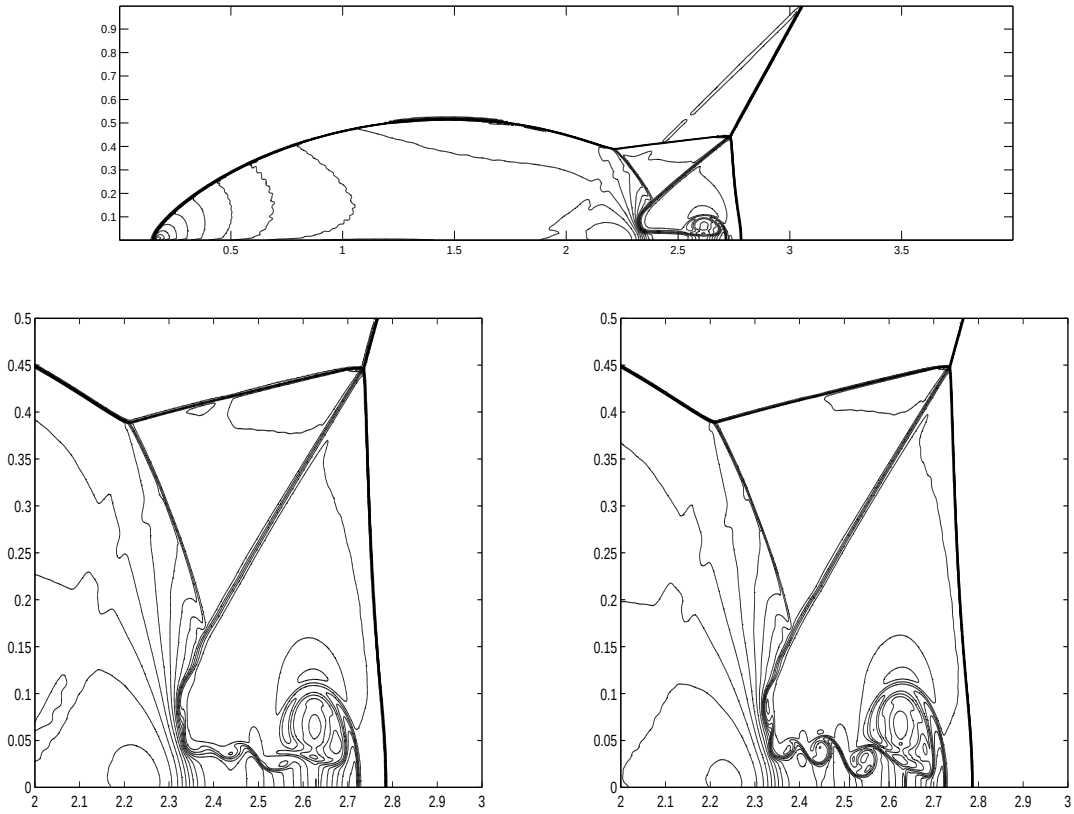

Figure 14: Density contour of the double Mach reflection. Computed on an irregular mesh (such that for one class of cells, $\Delta x = \Delta y = h$ in the upper half domain and $\Delta x = 2\Delta y = h$ in the lower half domain) by the 4th order central (Sec.2.2.2, 4 and (4.3)). Top: $h = 1/240$. Bottom left: $h = 1/400$. Bottom right: $h = 1/480$.

[13] A. Harten, *High resolution schemes for hyperbolic conservation laws*, J. Comput. Phys., 49 (1983), pp. 357–393.

[14] A. Harten, B. Engquist, S. Osher, and S. R. Chakravarthy, *Uniformly high order accuracy essentially non-oscillatory schemes III*, J. Comput. Phys., 71 (1987), pp. 231–303.

[15] C. Hu and C.-W. Shu, *Weighted essentially non-oscillatory schemes on triangular meshes*, J. Comput. Phys., 150 (1999), pp. 97–127.

[16] G.-S. Jiang, D. Levy, C.-T. Lin, S. Osher, and E. Tadmor, *High-resolution non-oscillatory central schemes with non-staggered grids for hyperbolic conservation laws*, SIAM J. Numer. Anal., 35 (1998), p. 2147.

[17] G.-S. Jiang and C.-W. Shu, *Efficient implementation of weighted ENO schemes*, J. Comput. Phys., 126 (1996), pp. 202–228.

[18] G.-S. Jiang and E. Tadmor, *Non-oscillatory central schemes for multidimensional hyperbolic conservation laws*, SIAM J. Sci. Comput., 19 (1998), pp. 1892–1917.

[19] A. Kurganov and D. Levy, *A third-order semi-discrete central scheme for conservation laws and convection-diffusion equations*, SIAM J. Sci. Comput., 22 (2000), pp. 1461–1488.

[20] A. Kurganov, S. Noelle, and G. Petrova, *Semidiscrete central-upwind schemes for hyperbolic conservation laws and Hamilton-Jacobi equations*, SIAM J. Sci. Comput., 23 (2001), pp. 707–740.

[21] A. Kurganov and E. Tadmor, *New high-resolution central schemes for nonlinear conservation laws and convection-diffusion equations*, J. Comput. Phys., 160 (2000), pp. 241–282.

[22] ———, *Solution of two-dimensional riemann problems for gas dynamics without riemann problem solvers*, Numerical Methods for Partial Differential Equations, 18 (2002), pp. 548–608.

[23] P. Lax and X.-D. Liu, *Solution of two dimensional riemann problem of gas dynamics by positive schemes*, SIAM J. Sci. Comput., 19 (1998), pp. 319–340.

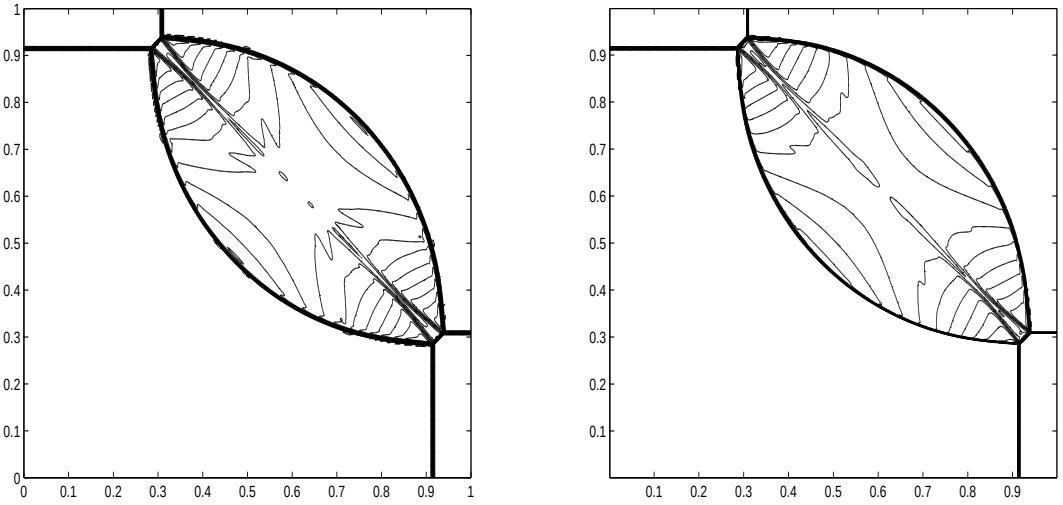

Figure 15: Density contour of a 2D Riemann problem [23]. Left: 5th order finite difference (Sec.3.3, 4 and (4.3)), $\Delta x = \Delta y = 1/400$. Right: 4th order central (Sec.2.2.2, 4 and (4.3)) on an irregular overlapping mesh such that for one class of the cells, $\Delta x = \Delta y = 1/400$ in the upper half domain and $\Delta x = 2\Delta y = 1/400$ in the lower half domain

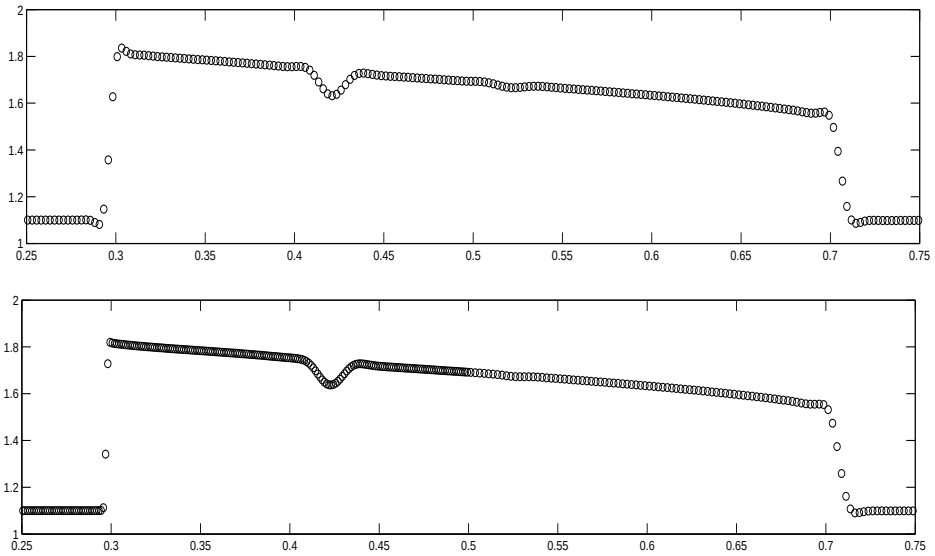

Figure 16: 2D Riemann problem [23]. Density along the line $x = 0.8$. Top: 5th order finite difference (Sec.3.3, 4 and (4.3)). Bottom: 4th order central (Sec.2.2.2, 4 and (4.3)) on the irregular overlapping mesh.

[24] D. Levy, G. Puppo, and G. Russo, *A fourth-order central WENO scheme for multidimensional hyperbolic systems of conservation laws*, SIAM J. Sci. Comput., 24 (2002), pp. 480–506.

[25] X. D. Liu, S. Osher, and T. Chan, *Weighted essentially non-oscillatory schemes*, J. Comput. Phys., 115 (1994), pp. 408–463.

[26] X.-D. Liu and E. Tadmor, *Third order nonoscillatory central scheme for hyperbolic conservation laws*, Numer. Math., 79 (1998), pp. 397–425.

[27] Y. Liu, *Central schemes on overlapping cells*, J. Comput. Phys., 209 (2005), pp. 82–104.
[28] Y. Liu, C.-W. Shu, E. Tadmor, and M. Zhang, *Central discontinuous Galerkin methods on overlapping cells with a non-oscillatory hierarchical reconstruction*, SIAM J. Numer. Anal., submitted.
[29] H. Nessyahu and E. Tadmor, *Non-oscillatory central differencing for hyperbolic conservation laws*, J. Comput. Phys., 87 (1990), pp. 408–463.
[30] J. Qiu and C.-W. Shu, *On the construction, comparison, and local characteristic decomposition for high-order central WENO schemes*, J. Comput. Phys., 183 (2002), pp. 187–209.
[31] ———, *Hermite WENO schemes and their application as limiters for Runge-Kutta discontinuous galerkin method. II. two dimensional case.*, Comput. & Fluids, 34 (2005), pp. 642–663.
[32] ———, *Runge-Kutta discontinuous Galerkin method using WENO limiters*, SIAM J. Sci. Comput., 26 (2005), pp. 907–929.
[33] A. M. Rogerson and E. Meiburg, *A numerical study of the convergence properties of ENO schemes*, J. Sci. Comput., 5 (1990), pp. 151–167.
[34] R. Sanders and A. Weiser, *High resolution staggered mesh approach for nonlinear hyperbolic systems of conservation laws*, J. Comput. Phys., 101 (1992), pp. 314–329.
[35] C.-W. Shu, *Numerical experiments on the accuracy of ENO and modified ENO schemes*, J. Sci. Comput., 5 (1990), pp. 127–149.
[36] ———, *Essentially non-oscillatory and weighted essentially non-oscillatory schemes for hyperbolic conservation laws*, Advanced Numerical Approximation of Nonlinear Hyperbolic Equations, A. Quarteroni, ed., Lecture Notes in Math.,Springer, Berlin., 1697 (1998).
[37] C.-W. Shu and S. Osher, *Efficient implementation of essentially non-oscillatory shock-capturing schemes*, J. Comput. Phys., 77 (1988), pp. 439–471.
[38] ———, *Efficient implementation of essentially nonoscillatory shock-capturing schemes, II*, J. Comput. Phys., 83 (1989), pp. 32–78.
[39] H.-Z. Tang and T. Tang, *Adaptive mesh methods for one- and two-dimensional hyperbolic conservation laws*, SIAM J. Numer. Anal., 41 (2003), pp. 487–515.
[40] B. van Leer, *Towards the ultimate conservative difference scheme II. monotonicity and conservation combined in a second order scheme*, J. Comput. Phys., 14 (1974), pp. 361–370.
[41] P. Woodward and P. Colella, *The numerical simulation of two-dimensional fluid flow with strong shocks*, J. Comput. Phys., 54 (1984), pp. 115–173.

(Yingjie Liu)
School of Mathematics
Georgia Institute of Technology
Atlanta, GA 30332-0160
E-mail address: yingjie@math.gatech.edu
URL: http://www.math.gatech.edu/~yingjie/

(Chi-Wang Shu)
Division of Applied Mathematics
Brown University
Providence RI 02912
E-mail address: shu@dam.brown.edu
URL: http://www.dam.brown.edu/people/shu/

(Eitan Tadmor)
Department of Mathematics, Institute for Physical Science and Technology
and Center of Scientific Computation And Mathematical Modeling (CSCAMM)
University of Maryland
College Park, MD 20742 USA
E-mail address: tadmor@cscamm.umd.edu
URL: http://www.cscamm.umd.edu/people/faculty/tadmor

(Mengping Zhang)
Department of Mathematics
University of Science and Technology of China
Hefei, Anhui 230026, China
E-mail address: mpzhang@ustc.edu.cn